A SMAD1/5-YAP signaling module drives radial glial cell expansion and growth of the developing cerebral cortex

Sonia Najas[1,2], Isabel Pijuan[1,2], Anna Esteve-Codina[3], Susana Usieto[1], Juan D. Martinez[1], An Zwijsen[4], Maria L. Arbonés[1,2], Elisa Martí[1] and Gwenvael Le Dréau[1,*]

[1] Department of Developmental Biology, Instituto de Biología Molecular de Barcelona, CSIC, Parc Científic de Barcelona, C/ Baldiri Reixac 10-15, 08028 Barcelona, Spain.

[2] Centro de Investigación Biomédica en Red de Enfermedades Raras (CIBERER), Barcelona, Spain.

[3] CNAG-CRG, Centre for Genomic Regulation (CRG), Barcelona Institute of Science and Technology (BIST), Baldiri i Reixac 4, 08028 Barcelona, Spain; Universitat Pompeu Fabra (UPF), Barcelona, Spain.

[4] Department of Cardiovascular Sciences, KU Leuven, Leuven 3000, Belgium.

[*] Author for correspondence: gldbmc@ibmb.csic.es

Key words (3-6): cerebral cortex; neurogenesis; radial glial cells; Bone morphogenetic proteins (BMPs); SMAD transcription factors; YAP.

Word count (main text, <7,000): 4,713

Running title (<35 characters): SMAD1/5 drives RGC self-amplification

Abstract

The growth and evolutionary expansion of the cerebral cortex are defined by the spatial-temporal production of neurons, which itself depends on the decision of radial glial cells (RGCs) to self-amplify or to switch to neurogenic divisions. The mechanisms regulating these RGC fate decisions are still incompletely understood. Here we describe a novel and evolutionarily conserved role of the canonical BMP transcription factors SMAD1/5 in controlling neurogenesis and growth during corticogenesis. Reducing the expression of both SMAD1 and SMAD5 in neural progenitors at early mouse cortical development caused microcephaly and an increased production of early-born cortical neurons at the expense of late-born ones, which correlated with the premature differentiation and depletion of the pool of cortical progenitors. Gain- and loss-of-function experiments performed during early cortical neurogenesis in the chick revealed that SMAD1/5 activity supports self-amplifying RGC divisions and restrain the neurogenic ones. Furthermore, we demonstrate that SMAD1/5 stimulate RGC self-amplification through the positive post-transcriptional regulation of the Hippo signaling effector YAP. We anticipate this SMAD1/5-YAP signaling module to be fundamental in controlling growth and evolution of the amniote cerebral cortex.

Introduction

The cerebral cortex is the region of the human brain responsible for higher cognitive functions. Errors during its formation provoke a vast array of brain disorders that affect intellectual ability and social behaviour (Hu et al., 2014; Jayaraman et al., 2018). This highlights the relevance of identifying the mechanisms that govern cortical development, in particular those controlling its growth and the production of neurons from cortical stem and progenitor cells.

Emerging in the dorsal part of the telencephalon (pallium), the mammalian cerebral cortex first consists of a pseudo-stratified epithelial layer (also called the ventricular zone, VZ) formed by primitive neural stem cells, the neuroepithelial cells, that rapidly mature into radial glial cells (RGCs) (Taverna et al., 2014). Like neuroepithelial cells, RGCs contact both the ventricle and the basal lamina, they divide at the apical membrane and they can expand through self-amplifying divisions that produce two daughter RGCs (De Juan Romero and Borrell, 2015; Taverna et al., 2014). Neurogenesis is initiated when RGCs start producing daughter cells committed to the neuronal lineage. Neurogenesis can occur directly, when a RGC divides asymmetrically to generate another RGC and a daughter cell that differentiates directly into a neuron (De Juan Romero and Borrell, 2015; Taverna et al., 2014). Alternatively, neurogenesis can be indirect, whereby a RGC gives rise to a RGC and a basal progenitor (BP) that harbours a restricted lineage potential, delaminates from the VZ and divides basally. These BPs will increase the neuronal output, possibly self-amplifying for several rounds of divisions before generating two neurons through a final self-consuming division (Lui et al., 2011). While intermediate progenitor cells (IPCs) possess a very limited self-amplifying potential and represent the vast majority of cortical BPs in lissencephalic species, basal (or outer) RGCs harbour a considerable self-amplifying potential and they

are responsible for the tremendous production of neurons and the larger neocortex observed in gyrencephalic species (Lui et al., 2011; Shitamukai et al., 2011; Wang et al., 2011). Therefore, the decision of a RGC to self-amplify or to give rise to neurons, either directly or indirectly, has a huge impact on the final number of neurons in the cerebral cortex.

As highlighted by the gene mutations causing primary microcephaly, a variety of intracellular events regulate cerebral cortical size, including centrosome behaviour and centriole biogenesis, DNA replication and repair, cytokinesis and apical-basal polarity (Jayaraman et al., 2018; Saade et al., 2018). Moreover, the balance between RGC self-amplification and neurogenesis appears to be regulated by extrinsic cues emanating from the ventricular fluid, meninges, blood vessels and neighbouring cells (Llinares-Benadero and Borrell, 2019; Martynoga et al., 2012; Taverna et al., 2014). Thus, the molecular events regulating RGC fate are complex and they are still not fully understood.

Seminal studies performed on cortical progenitors *in vitro* suggested that Bone morphogenetic protein (BMP) signaling regulates their neurogenic potential (Li et al., 1998; Mabie et al., 1999). The microcephaly described in *Bmp7* mutant mice, and the over-proliferation and premature differentiation reported in the brains of transgenic mice expressing constitutively active forms of the type-1 BMP receptors *Alk3/Bmpr1a* or *Alk6/Bmpr1b* supported this idea (Panchision et al., 2001; Segklia et al., 2012). However, definitive proofs of an instructive role for BMP signaling in cortical RGC fate decision *in vivo* are still lacking.

Here we found that the activity of the transcription factors SMAD1/5, two canonical effectors of BMP signalling, promotes cortical RGC self-amplification in both chick and mouse embryos, preventing their premature neurogenic switch and exhaustion, and

thereby ensuring the appropriate production of the distinct classes of cortical excitatory neurons. In searching for the effectors of SMAD1/5 activity, we show that this role depends on the post-transcriptional regulation of YAP, a core component of the Hippo signaling pathway known to regulate cell growth and organ size (Yu et al., 2015). Together, our findings reveal an instructive and evolutionarily conserved role of the canonical BMP effectors SMAD1/5 in the control of RGC self-amplification in the developing cerebral cortex.

Results

SMAD1/5 activity is required for brain growth and cortical neurogenesis in mouse.

To determine the role played by the canonical BMP pathway during mammalian cerebral cortex development, we focused on the function of its canonical effectors SMAD1/5/8 during mouse corticogenesis. *In situ* hybridization revealed that *mSmad1* and *mSmad5* transcripts are expressed throughout the rostral-caudal axis of the developing mouse cerebral cortex at embryonic day (E) 14.5 and are particularly enriched in the VZ, whereas *mSmad8* transcripts were not detected (Fig.1A). In agreement with previous observations (Saxena et al., 2018), immunostaining at mid-corticogenesis with an antibody that specifically recognizes the active, carboxy-terminal phosphorylated form of SMAD1/5/8 (pSMAD1/5/8) revealed activity of these canonical BMP effectors in differentiating neurons as well as in both apically- and basally-dividing cortical progenitors (Fig.1B). When quantified in $pH3^{+}$ mitotic nuclei, pSMAD1/5/8 immunostaining revealed SMAD1/5 activity to be stronger in apically-dividing mouse RGCs than in basally-dividing IPCs (Fig.1C), suggesting a correlation between high SMAD1/5 activity and RGC maintenance.

To understand the role played by SMAD1/5 during mouse cerebral cortex development, we crossed $Smad1^{fl/fl};Smad5^{fl/fl}$ mice (Moya et al., 2012) with a *Nestin:cre* transgenic line that produces Cre-mediated recombination in neural progenitor cells and somites as early as E8.5 (Petersen et al., 2002), in contrast to the more commonly used *Nestin:cre* transgenic line that produces efficient Cre-mediated recombination in cortical progenitors from mid-embryogenesis (Liang et al., 2012). In agreement with the early Cre-mediated recombination expected from this *Nestin:cre* transgenic line (Moya et al., 2012; Petersen et al., 2002), SMAD1 and SMAD5 protein levels were reduced by

54% and 32% in telencephalic extracts from E11.5 Smad1$^{wt/fl}$;Smad5$^{wt/fl}$;Nestin:Cre$^{+/0}$ heterozygous embryos relative to their control Smad1$^{wt/fl}$;Smad5$^{wt/fl}$;Nestin:Cre$^{0/0}$ littermates (Fig.S1). These Smad1$^{wt/fl}$;Smad5$^{wt/fl}$;Nestin:Cre$^{+/0}$ heterozygous mutant mice were viable and born following Mendelian ratios but were sterile, precluding the study of the homozygous mutants. Interestingly, the adult (P60) Smad1$^{wt/fl}$;Smad5$^{wt/fl}$;Nestin:Cre$^{+/0}$ heterozygous mutant mice (hereafter referred to as SmadNes mutants or +/-) presented a smaller brain than their control littermates (Fig.1D), including reductions in brain weight (0.544g ± 0.021 for controls *vs* 0.407g ± 0.006 for SmadNes mutants; Fig.1E) and brain size (4.404 ± 0.147 x10^7 µm^2 for controls *vs* 3.780 ± 0.113 x10^7 µm^2 for SmadNes mutants, Fig.1F,G). These reductions in brain weight and size were both greater than 3SD, implying according to clinical standards that the SmadNes heterozygous mutants suffer a severe microcephaly (Passemard et al., 2013). The size reduction of the adult SmadNes mutant brain was constant across the rostral-caudal axis (Fig.S2A,B), suggesting that SMAD1/5 inhibition impaired growth equally in all brain regions. Apart from these growth defects and a thinner corpus callosum (Fig.S2A,C), the brain of the SmadNes mutants did not present any major neuro-anatomical defects (Fig.1F and Fig.S2A). Intriguingly, the neocortex of adult SmadNes mutants did not appear to have fewer neurons per radial column unit (332.8 ± 16.8 NeuN$^+$ cells per 100µm for controls *vs* 332.8 ± 14.1 for SmadNes mutants), but the relative proportions of its neuronal layers were altered (Fig.1H-J). The number of early-born neurons forming the deep layer L6 and its thickness were increased, whereas these parameters were diminished in the superficial L2/3 layer containing late-born callosal projection neurons (Fig.1H-J), consistent with the reduced thickness of the corpus callosum (Fig.S2). This phenotype was observed at

the early postnatal stage P7 (Fig.1K-M), supporting the idea that these cortical defects originated during the embryonic phase.

While the SmadNes mutant embryos did not present any obvious defect in telencephalic patterning (Fig.S3), their programme of cortical neurogenesis did appear to be altered (Fig.2). Around the onset of cortical neurogenesis (E11.5), the SmadNes mutant embryos had correct numbers of RGCs ($PAX6^+$;$TBR2^-$ cells) and IPCs ($TBR2^+$ cells) per radial unit, yet their neuronal output was increased (Fig.2A-F). Accordingly, there were more early-born differentiating $TBR1^+$ neurons in the SmadNes mutant cortex than in their control littermates from E11.5 onwards (Fig.2G,H). The developing cerebral cortex of the SmadNes mutant embryos contained fewer IPCs from E13.5 onwards and fewer RGCs at E17.5 (Fig.2B-D). This decrease in cortical progenitors at E17.5 was associated with a lower neuronal output and fewer late-born $SATB2^+$ neurons (Fig.2E,F,I,J). Together, these data confirmed the developmental origin of the cortical alterations seen in the cerebral cortex of P7 and P60 SmadNes mutants (Fig.1H-M). The mitotic indices of the cortical RGCs and IPCs were comparable in SmadNes mutants and controls at all stages examined (Fig.S4), suggesting that the proliferation rate of the cortical progenitors is not severely affected in SmadNes mutants. We thus reasoned that the increased production of early-born neurons, the premature reduction in the number of RGCs and IPCs and the decreased production of late-born neurons observed in the cerebral cortex of SmadNes heterozygous mutant embryos might likely be the result of a premature switch of RGCs from self-amplifying to neurogenic divisions during early corticogenesis.

SMAD1/5 activity is required for RGC self-amplification during chick cortical neurogenesis.

There is increasing evidence that the basic gene regulatory networks, progenitor cell types and cellular events governing the generation of neurons during corticogenesis are evolutionarily conserved between mammals and sauropsids, particularly birds (Cardenas et al., 2018; Le Dreau et al., 2018; Nomura et al., 2013; Suzuki et al., 2012; Yamashita et al., 2018). To assess whether SMAD1/5 regulate the mode of division of cortical RGCs, we turned to the developing chick cerebral cortex, as this avian model offered greater possibilities than the mouse to accurately manipulate SMAD1/5 activity at the onset of cortical neurogenesis.

The production of neurons in the PAX6^{+} developing chick cerebral cortex spans from E3 to E8 (Fig.3A,B; Suzuki et al., 2012). As in mammals (Taverna et al., 2014), cortical neurogenesis in the chick is initiated by the onset of neurogenic divisions of PAX6^{+};TBR2^{-} RGCs that divide apically in the VZ (Fig.3A,B). From E5 onwards, the production of cortical neurons is enhanced by symmetric neurogenic divisions of basally-dividing TBR2^{+} IPCs (Fig.3A,B; Suzuki et al., 2012). *In situ* hybridization revealed that both *cSmad1* and *cSmad5* transcripts are expressed throughout the neurogenic period, mostly in the VZ where *cSmad8* transcripts were essentially absent (Fig.S5). Immunostaining with the pSMAD1/5/8 antibody at E5 revealed activity of SMAD1/5 in both apically- and basally-dividing cortical progenitors as well as in differentiating neurons (Fig.3C), as previously observed in the developing mouse cortex (Fig.1B). When quantified in pH3^{+} mitotic nuclei, SMAD1/5 activity was weaker in basal IPC divisions than in RGC divisions (Fig.3D). When quantified after *in ovo* electroporation of a pTis21:RFP reporter that is specifically activated during neurogenic divisions (Fig.S6; Le Dreau et al., 2014; Saade et al., 2017; Saade et al., 2013),

SMAD1/5 activity was diminished in pTis21:RFP$^+$ neurogenic divisions relative to pTis21:RFP$^-$ self-amplifying divisions (Fig.3E,F). Therefore, a positive correlation exists between SMAD1/5 activity and the potential for RGC self-amplification during chick cortical neurogenesis.

Endogenous SMAD1/5 activity was inhibited from the onset of cortical neurogenesis by *in ovo* electroporation of sh-RNA plasmids that specifically target *cSmad1* or *cSmad5* (sh-S1/5; Le Dreau et al., 2012). Inhibiting SMAD1 or SMAD5 activity resulted in a similar phenotype, nearly doubling the proportion of electroporated RGCs undergoing neurogenic pTis21:RFP$^+$ divisions (Fig.3G,H). This precocious switch to neurogenic divisions provoked a premature and accelerated depletion of electroporated PAX6$^+$;TBR2$^-$ RGCs, their accelerated progression towards a committed TBR2$^+$ fate and ultimately, their differentiation into SOX2$^-$;HuC/D$^+$ and TBR1$^+$ neurons (Fig.3I-K). Thus, full SMAD1/5 activity is required to support RGC self-amplification during chick cortical neurogenesis.

Conversely, enhancing canonical BMP activity through *in ovo* electroporation of a constitutively active SMAD5 mutant (SMAD5-S/D; Le Dreau et al., 2012) produced the opposite phenotype, a 2-fold reduction in the proportion of electroporated RGCs undergoing neurogenic pTis21:RFP$^+$ divisions (Fig.4A,B). This reduction in neurogenic divisions was associated with the electroporated cells remaining as PAX6$^+$;TBR2$^-$ RGCs and it impeded their transition into the neuronal lineage (Fig.4C,D). Notably, the SMAD5-S/D construct rescued the phenotype caused by sh-S5 (Fig.4E,F). In 5 out of 20 electroporated embryos, SMAD5-S/D electroporation itself caused the abnormal generation of ectopic rosettes of cortical progenitors, which developed an apical-basal polarity (Fig.S7). Together, these data revealed that the fine tuning of SMAD1/5

activity is required to properly balance the self-amplification of RGCs with the production of cortical excitatory neurons.

SMAD1/5 regulate RGC self-amplification and early cortical neurogenesis through YAP.

To identify the gene regulatory networks controlled by SMAD1/5 during cortical neurogenesis, cortical RGCs from SmadNes mutant and control E12.5 embryos were purified by FACS based on their Prominin1 expression (Corti et al., 2007), and their transcriptomes were compared by genome-wide RNA-sequencing (Fig.5A). A short list of differentially expressed transcripts (DETs) was identified (90 DETs with adj $p<0.05$ and 128 with adj $p<0.1$: Fig.5B and Table S1). A gene ontology (GO) term enrichment analysis correlated this DET signature to the regulation of neurogenesis and cell biosynthesis (Fig.5C). A Transfac/Jaspar analysis revealed that the promoter regions of these DETs are enriched in binding motifs for transcription factors of the TEAD and SP families (Fig.5D). We considered particularly interesting these latter results pointing to an altered TEAD activity in response to SMAD1/5 inhibition. The TEAD TFs indeed represent the transcriptional effectors of the Hippo signalling pathway, which regulates cell growth and organ size (Yu et al., 2015). The activity of TEADs depends directly on the availability of their co-factors YAP/TAZ, which are themselves regulated by upstream kinases of the Hippo pathway (Yu et al., 2015). However, we did not observe any alteration in the transcript levels of the TEAD TFs expressed in mouse cortical RGCs in response to SMAD1/5 inhibition, nor of other factors known to participate in Hippo signalling (Table S2). Thereby, SMAD1/5 does not appear to regulate any member of the Hippo signalling pathway at the transcriptional level.

Previous findings established that YAP can physically interact with SMAD1/5 and that its activity is required for optimal SMAD1/5 activity in several cellular contexts, including cultured mouse embryonic stem cells, the drosophila wing imaginal disc and during postnatal mouse astrocyte differentiation (Fig.6A; Alarcon et al., 2009; Huang et al., 2016). On the other hand, BMP-induced SMAD1/5 signalling has been reported to stimulate YAP protein stability and activity (Fig.6A; Huang et al., 2016). We thus reasoned that YAP might participate together with SMAD1/5 in controlling RGC self-amplification during cortical neurogenesis. Therefore, we analysed YAP expression and activity relative to SMAD1/5 activity during cortical neurogenesis. In agreement with recent reports (Kostic et al., 2019; Saito et al., 2018), immunostaining for the YAP protein revealed that the active (nuclear) YAP was more intensely expressed in apically-dividing RGCs than in basally-dividing IPCs, and this profile was strongly correlated with SMAD1/5 activity during both chick and mouse cortical neurogenesis (Fig.6B-E and S8A-D). Inhibiting SMAD1/5 during chick cortical neurogenesis impaired YAP activity, as witnessed through the reduced nuclear YAP intensity and the increase in the phosphorylated form of YAP (pYAP) primed for proteasomal degradation relative to the total YAP (Fig.6F,G and S8E,F). Similarly, the pYAP/YAP ratio increased in the cortex of E11.5 SmadNes mutant embryos (Fig.6H,I and S8G,H). These latter findings indicate that SMAD1/5 positively regulate YAP protein levels and activity both during mouse and chick cortical neurogenesis.

Finally, we tested whether increasing YAP activity could compensate for the phenotype caused by SMAD1/5 inhibition. *In ovo* electroporation of a wild type form of YAP rescued the premature exhaustion of RGCs driven by sh-S1, reverting it to control levels and impeding their differentiation into $SOX2^{-}$;HuC/D^{+} neurons (Fig.6J-N). Intriguingly, YAP overexpression forced the vast majority of electroporated cells to

remain SOX2^{+} (Fig.6J,K), with more than 30% being found ectopically in the mantle zone irrespective of SMAD1 inhibition (Fig.6J,N and S8I). Together, these results support a model whereby SMAD1/5 promotes RGC self-amplification and orchestrate cortical neurogenesis through YAP (Fig.6O).

Discussion

In this study, we identify a novel role for the canonical BMP effectors SMAD1/5 in cortical neurogenesis. The results obtained in the developing chick cerebral cortex demonstrated that their activity stimulates RGC self-amplification and impedes their premature switch to neurogenic divisions. Reducing SMAD1/5 activity during early mouse corticogenesis caused cortical progenitors to prematurely enter neurogenesis, enhancing the generation of early-born cortical neurons and prematurely exhausting the RGC and IPC pools, subsequently limiting the production of late-born cortical neurons. As such, the role of SMAD1/5 in promoting RGC maintenance appears to be conserved in mammalian corticogenesis. Therefore, our results strongly suggest that the dependence on SMAD1/5 activity to maintain RGC self-amplification and ensure the appropriate production of excitatory neurons during corticogenesis is evolutionarily conserved in amniotes, at least between mammals and birds. This leads us to hypothesize that BMP signaling through its canonical effectors SMAD1/5 is part of the core ancestral gene regulatory network that governs corticogenesis throughout the amniote lineage, together with PAX6, the proneural bHLH proteins and the NOTCH and SLIT/ROBO signalling pathways (Cardenas et al., 2018; Le Dreau et al., 2018; Nomura et al., 2013; Suzuki et al., 2012; Yamashita et al., 2018).

Notably, the cerebral cortex of adult SmadNes mutant mice is smaller along the medial-lateral and rostral-caudal axes, although its thickness and the number of neurons in the radial columns are nearly normal. These observations suggest that reducing SMAD1/5 activity affects more severely the generation of radial columns than the number of cells per radial unit, emphasizing the importance of SMAD1/5 activity for cortical RGC self-amplification, which represents a critical step in the regulation of the growth of the cerebral cortex and which is particularly crucial before and during the

early stages of cortical neurogenesis (Cardenas and Borrell, 2019). Crossing the Smad1$^{fl/fl}$;Smad5$^{fl/fl}$ mice with the Nestin:cre line from Jackson Laboratory, which produces an efficient Cre-mediated recombination in cortical progenitors only from late embryogenesis (around E17.5, Liang et al., 2012), did not cause any obvious alteration in cortical neurogenesis nor any apparent brain growth defects (Dr Eve Seuntjens, unpublished observations). These observations further support our conclusion that the role of SMAD1/5 in sustaining RGC self-amplification is especially crucial during the early steps of cortical neurogenesis.

Since the SmadNes heterozygous mutant mice present an overall reduction in brain size and weight, it is likely that SMAD1/5 play a similar role throughout the developing brain. Alterations of SMAD1/5 activity are also likely to underlie the microcephaly described in *Bmp7* mutant mice and the phenotype of excess proliferation in the brain of mice overexpressing a constitutively active form of the type-1 receptor *Alk3* (Panchision et al., 2001; Segklia et al., 2012). Our present findings are also in agreement with the previous demonstration that SMAD1/5 promote neural progenitor self-amplification during spinal neurogenesis (Le Dreau et al., 2018; Le Dreau et al., 2014). Altogether, these data thus suggest that canonical BMP signalling through SMAD1/5 regulates stem cell maintenance and growth throughout the developing CNS.

A crucial role of SMAD1/5 in growth control during CNS development is further supported by our data showing that SMAD1/5 regulate YAP activity in early cortical RGCs. As a central element in the Hippo signaling pathway, YAP plays a fundamental role in the control of cell growth and of organ size in many tissues (Yu et al., 2015). Accordingly, the tight regulation of YAP activity appears to be crucial for correct brain formation and growth. Cortical and general brain development is affected when YAP activity is enhanced, either directly or indirectly (Lavado et al., 2013; Lavado et al.,

2018; Liu et al., 2018; Saito et al., 2018). More importantly, an aberrant increase in YAP activity has been linked to various types of cortical heterotopia, such as those observed in the Van Maldergem syndrome (Cappello et al., 2013; Liu et al., 2018). Our observation that YAP overexpression causes ribbon-like heterotopias of $SOX2^+$ and $PAX6^+$ progenitors in the developing chick cerebral cortex is therefore reminiscent of these severe mammalian cortical defects. Conversely, a reduction in YAP activity is plausibly one of the mechanistic events contributing to primordial dwarfism syndromes, whose defining features include microcephaly and general growth defects (Klingseisen and Jackson, 2011). Of note, the SmadNes heterozygous mutant mice presented microcephaly and growth retardation. Interestingly, the levels of YAP activity also determine the abundance and proliferative ability of neocortical basal progenitors (Kostic et al., 2019), such that its regulation might have contributed to the evolutionary diversification and expansion of the mammalian neocortex. Our findings suggest that the regulation of YAP activity by SMAD1/5 in RGCs might be evolutionarily conserved. It is thus tempting to speculate that modulations of the canonical BMP activity might have influenced the growth and expansion of the cerebral cortex during amniote evolution, an hypothesis that remains to be investigated further.

Acknowledgments

Acknowledgements: we thank the members of M.L.A's and E.M's laboratories for their discussion of this study. We thank E. Rebollo and the IBMB Molecular Imaging platform, J. Comas and the PCB Flow Cytometry facility, and the CNAG-CRG Sequencing Unit for their assistance. We are grateful to E.J. Robertson and W. Zhong for providing the *Smad1*$^{fl/fl}$ and *Nestin:cre* mice, and to E. Seuntjens for sharing information. **Funding:** the work in M.L.A's and E.M's laboratories was supported by the grants SAF2016-77971-R, BFU2016-81887-REDT and BFU2016-77498-P. I.P. received a PhD fellowship from the Spanish Ministry of Economy, Industry and Competitiveness (MINEICO, BES2014-069217). A. E-C was supported by ISCIII (MINEICO, PT17/0009/0019) and the Fondo Europeo de Desarrollo Regional (FEDER). G.L.D. was supported by the AECC (AIO2014). **Author contributions:** Conceptualization: S.N. and G.L.D.; Methodology: S.N., I.P., A.E-C., S.U., J.D.M. and G.L.D.; Investigation: S.N., I.P., A.E-C. and G.L.D.; Resources: A.Z., M.L.A and E.M; Visualization: G.L.D.; Writing - Original Draft: G.L.D.; Funding Acquisition: M.L.A. and E.M.; Supervision: M.L.A., E.M. and G.L.D. **Competing interests:** the authors have no competing financial interests to declare. **Data and materials availability:** All data is available in the main text or supplemental information. **Correspondence and requests for materials** should be addressed to G.L.D.

References

Alarcon, C., Zaromytidou, A. I., Xi, Q., Gao, S., Yu, J., Fujisawa, S., Barlas, A., Miller, A. N., Manova-Todorova, K., Macias, M. J. et al. (2009). Nuclear CDKs drive Smad transcriptional activation and turnover in BMP and TGF-beta pathways. *Cell* 139, 757-69.

Cappello, S., Gray, M. J., Badouel, C., Lange, S., Einsiedler, M., Srour, M., Chitayat, D., Hamdan, F. F., Jenkins, Z. A., Morgan, T. et al. (2013). Mutations in genes encoding the cadherin receptor-ligand pair DCHS1 and FAT4 disrupt cerebral cortical development. *Nat Genet* 45, 1300-8.

Cardenas, A. and Borrell, V. (2019). Molecular and cellular evolution of corticogenesis in amniotes. *Cell Mol Life Sci*.

Cardenas, A., Villalba, A., de Juan Romero, C., Pico, E., Kyrousi, C., Tzika, A. C., Tessier-Lavigne, M., Ma, L., Drukker, M., Cappello, S. et al. (2018). Evolution of Cortical Neurogenesis in Amniotes Controlled by Robo Signaling Levels. *Cell* 174, 590-606 e21.

Corti, S., Nizzardo, M., Nardini, M., Donadoni, C., Locatelli, F., Papadimitriou, D., Salani, S., Del Bo, R., Ghezzi, S., Strazzer, S. et al. (2007). Isolation and characterization of murine neural stem/progenitor cells based on Prominin-1 expression. *Exp Neurol* 205, 547-62.

Chen, E. Y., Tan, C. M., Kou, Y., Duan, Q., Wang, Z., Meirelles, G. V., Clark, N. R. and Ma'ayan, A. (2013). Enrichr: interactive and collaborative HTML5 gene list enrichment analysis tool. *BMC Bioinformatics* 14, 128.

De Juan Romero, C. and Borrell, V. (2015). Coevolution of radial glial cells and the cerebral cortex. *Glia* 63, 1303-19.

Dobin, A., Davis, C. A., Schlesinger, F., Drenkow, J., Zaleski, C., Jha, S., Batut, P., Chaisson, M. and Gingeras, T. R. (2013). STAR: ultrafast universal RNA-seq aligner. *Bioinformatics* 29, 15-21.

Hamburger, V. and Hamilton, H. L. (1951). A series of normal stages in the development of chick embryo. *J. Morphol.* 88, 49-92.

Hu, W. F., Chahrour, M. H. and Walsh, C. A. (2014). The diverse genetic landscape of neurodevelopmental disorders. *Annu Rev Genomics Hum Genet* 15, 195-213.

Huang, Z., Hu, J., Pan, J., Wang, Y., Hu, G., Zhou, J., Mei, L. and Xiong, W. C. (2016). YAP stabilizes SMAD1 and promotes BMP2-induced neocortical astrocytic differentiation. *Development* 143, 2398-409.

Jayaraman, D., Bae, B. I. and Walsh, C. A. (2018). The Genetics of Primary Microcephaly. *Annu Rev Genomics Hum Genet* 19, 177-200.

Klingseisen, A. and Jackson, A. P. (2011). Mechanisms and pathways of growth failure in primordial dwarfism. *Genes Dev* 25, 2011-24.

Kojima, S., Vignjevic, D. and Borisy, G. G. (2004). Improved silencing vector co-expressing GFP and small hairpin RNA. *Biotechniques* 36, 74-9.

Kostic, M., Paridaen, J., Long, K. R., Kalebic, N., Langen, B., Grubling, N., Wimberger, P., Kawasaki, H., Namba, T. and Huttner, W. B. (2019). YAP Activity Is Necessary and Sufficient for Basal Progenitor Abundance and Proliferation in the Developing Neocortex. *Cell Rep* 27, 1103-1118 e6.

Kuleshov, M. V., Jones, M. R., Rouillard, A. D., Fernandez, N. F., Duan, Q., Wang, Z., Koplev, S., Jenkins, S. L., Jagodnik, K. M., Lachmann, A. et al. (2016). Enrichr: a comprehensive gene set enrichment analysis web server 2016 update. *Nucleic Acids Res* 44, W90-7.

Lavado, A., He, Y., Pare, J., Neale, G., Olson, E. N., Giovannini, M. and Cao, X. (2013). Tumor suppressor Nf2 limits expansion of the neural progenitor pool by inhibiting Yap/Taz transcriptional coactivators. *Development* 140, 3323-34.
Lavado, A., Park, J. Y., Pare, J., Finkelstein, D., Pan, H., Xu, B., Fan, Y., Kumar, R. P., Neale, G., Kwak, Y. D. et al. (2018). The Hippo Pathway Prevents YAP/TAZ-Driven Hypertranscription and Controls Neural Progenitor Number. *Dev Cell* 47, 576-591 e8.
Le Dreau, G., Escalona, R., Fueyo, R., Herrera, A., Martinez, J. D., Usieto, S., Menendez, A., Pons, S., Martinez-Balbas, M. A. and Marti, E. (2018). E proteins sharpen neurogenesis by modulating proneural bHLH transcription factors' activity in an E-box-dependent manner. *Elife* 7.
Le Dreau, G., Garcia-Campmany, L., Rabadan, M. A., Ferronha, T., Tozer, S., Briscoe, J. and Marti, E. (2012). Canonical BMP7 activity is required for the generation of discrete neuronal populations in the dorsal spinal cord. *Development* 139, 259-68.
Le Dreau, G., Saade, M., Gutierrez-Vallejo, I. and Marti, E. (2014). The strength of SMAD1/5 activity determines the mode of stem cell division in the developing spinal cord. *J Cell Biol* 204, 591-605.
Levy, D., Adamovich, Y., Reuven, N. and Shaul, Y. (2008). Yap1 phosphorylation by c-Abl is a critical step in selective activation of proapoptotic genes in response to DNA damage. *Mol Cell* 29, 350-61.
Li, B. and Dewey, C. N. (2011). RSEM: accurate transcript quantification from RNA-Seq data with or without a reference genome. *BMC Bioinformatics* 12, 323.
Li, W., Cogswell, C. A. and LoTurco, J. J. (1998). Neuronal differentiation of precursors in the neocortical ventricular zone is triggered by BMP. *J Neurosci* 18, 8853-62.
Liang, H., Hippenmeyer, S. and Ghashghaei, H. T. (2012). A Nestin-cre transgenic mouse is insufficient for recombination in early embryonic neural progenitors. *Biol Open* 1, 1200-3.
Liu, W. A., Chen, S., Li, Z., Lee, C. H., Mirzaa, G., Dobyns, W. B., Ross, M. E., Zhang, J. and Shi, S. H. (2018). PARD3 dysfunction in conjunction with dynamic HIPPO signaling drives cortical enlargement with massive heterotopia. *Genes Dev* 32, 763-780.
Love, M. I., Huber, W. and Anders, S. (2014). Moderated estimation of fold change and dispersion for RNA-seq data with DESeq2. *Genome Biol* 15, 550.
Lui, J. H., Hansen, D. V. and Kriegstein, A. R. (2011). Development and evolution of the human neocortex. *Cell* 146, 18-36.
Llinares-Benadero, C. and Borrell, V. (2019). Deconstructing cortical folding: genetic, cellular and mechanical determinants. *Nat Rev Neurosci*.
Mabie, P. C., Mehler, M. F. and Kessler, J. A. (1999). Multiple roles of bone morphogenetic protein signaling in the regulation of cortical cell number and phenotype. *J Neurosci* 19, 7077-88.
Martynoga, B., Drechsel, D. and Guillemot, F. (2012). Molecular control of neurogenesis: a view from the mammalian cerebral cortex. *Cold Spring Harb Perspect Biol* 4.
Megason, S. G. and McMahon, A. P. (2002). A mitogen gradient of dorsal midline Wnts organizes growth in the CNS. *Development* 129, 2087-98.
Moya, I. M., Umans, L., Maas, E., Pereira, P. N., Beets, K., Francis, A., Sents, W., Robertson, E. J., Mummery, C. L., Huylebroeck, D. et al. (2012). Stalk cell phenotype depends on integration of Notch and Smad1/5 signaling cascades. *Dev Cell* 22, 501-14.
Nomura, T., Gotoh, H. and Ono, K. (2013). Changes in the regulation of cortical neurogenesis contribute to encephalization during amniote brain evolution. *Nat Commun* 4, 2206.

Panchision, D. M., Pickel, J. M., Studer, L., Lee, S. H., Turner, P. A., Hazel, T. G. and McKay, R. D. (2001). Sequential actions of BMP receptors control neural precursor cell production and fate. *Genes Dev* 15, 2094-110.
Passemard, S., Kaindl, A. M. and Verloes, A. (2013). Microcephaly. *Handb Clin Neurol* 111, 129-41.
Petersen, P. H., Zou, K., Hwang, J. K., Jan, Y. N. and Zhong, W. (2002). Progenitor cell maintenance requires numb and numblike during mouse neurogenesis. *Nature* 419, 929-34.
Saade, M., Blanco-Ameijeiras, J., Gonzalez-Gobartt, E. and Marti, E. (2018). A centrosomal view of CNS growth. *Development* 145.
Saade, M., Gonzalez-Gobartt, E., Escalona, R., Usieto, S. and Marti, E. (2017). Shh-mediated centrosomal recruitment of PKA promotes symmetric proliferative neuroepithelial cell division. *Nat Cell Biol* 19, 493-503.
Saade, M., Gutierrez-Vallejo, I., Le Dreau, G., Rabadan, M. A., Miguez, D. G., Buceta, J. and Marti, E. (2013). Sonic hedgehog signaling switches the mode of division in the developing nervous system. *Cell Rep* 4, 492-503.
Saito, K., Kawasoe, R., Sasaki, H., Kawaguchi, A. and Miyata, T. (2018). Neural Progenitor Cells Undergoing Yap/Tead-Mediated Enhanced Self-Renewal Form Heterotopias More Easily in the Diencephalon than in the Telencephalon. *Neurochem Res* 43, 180-189.
Saxena, M., Agnihotri, N. and Sen, J. (2018). Perturbation of canonical and non-canonical BMP signaling affects migration, polarity and dendritogenesis of mouse cortical neurons. *Development* 145.
Segklia, A., Seuntjens, E., Elkouris, M., Tsalavos, S., Stappers, E., Mitsiadis, T. A., Huylebroeck, D., Remboutsika, E. and Graf, D. (2012). Bmp7 regulates the survival, proliferation, and neurogenic properties of neural progenitor cells during corticogenesis in the mouse. *PLoS One* 7, e34088.
Shitamukai, A., Konno, D. and Matsuzaki, F. (2011). Oblique radial glial divisions in the developing mouse neocortex induce self-renewing progenitors outside the germinal zone that resemble primate outer subventricular zone progenitors. *J Neurosci* 31, 3683-95.
Suzuki, I. K., Kawasaki, T., Gojobori, T. and Hirata, T. (2012). The temporal sequence of the mammalian neocortical neurogenetic program drives mediolateral pattern in the chick pallium. *Dev Cell* 22, 863-70.
Taverna, E., Gotz, M. and Huttner, W. B. (2014). The cell biology of neurogenesis: toward an understanding of the development and evolution of the neocortex. *Annu Rev Cell Dev Biol* 30, 465-502.
Wang, X., Tsai, J. W., LaMonica, B. and Kriegstein, A. R. (2011). A new subtype of progenitor cell in the mouse embryonic neocortex. *Nat Neurosci* 14, 555-61.
Yamashita, W., Takahashi, M., Kikkawa, T., Gotoh, H., Osumi, N., Ono, K. and Nomura, T. (2018). Conserved and divergent functions of Pax6 underlie species-specific neurogenic patterns in the developing amniote brain. *Development* 145.
Yu, F. X., Zhao, B. and Guan, K. L. (2015). Hippo Pathway in Organ Size Control, Tissue Homeostasis, and Cancer. *Cell* 163, 811-28.

Figure Legends

Figure 1: inhibiting SMAD1/5 activity in mouse neural progenitors causes microcephaly and alters the numbers of early- and late-born neocortical neurons.

(A) Sagittal sections of the developing mouse dorsal telencephalon showing mSmad1, mSmad5 and mSmad8 transcripts at E14.5, obtained from Genepaint (https://gp3.mpg.de). (B) The pSMAD1/5/8 immunoreactivity at E13.5 and (C) its mean intensity ± s.d. measured in 144 apical and 64 basal mitoses obtained from 3 mouse E13.5 embryos. (D) Images, (E) mean weight ± s.d, (F) coronal sections of the brains of SmadNes mutant mice (+/-) and their control littermates (+/+) and (G) their surface area ± s.d at P60, obtained from 3-5 animals per genotype. (H) Neuronal layer organization, (I) mean thickness of the layers ± s.e.m and (J) mean number of neurons ± s.e.m in the different layers in radial units (100 µm) of the cerebral cortex of SmadNes mutant mice and their control littermates at P60, obtained from 3-4 animals per genotype. (K) Representative images of early-born $TBR1^+$ L6 and late-born $MEF2C^+$ L4-2/3 projection neurons, (L) mean thickness of the layers ± s.e.m and (M) mean number of neurons ± s.e.m in the different layers in radial units (200 µm) of the developing cerebral cortex of the SmadNes mutant pups and their control littermates at P7, obtained from 5-6 animals per genotype. Significance was assessed with the non-parametric Mann–Whitney test (C, E, G; I and L for the total cumulated thickness) or a two-way ANOVA + Sidak's test (I, J, L, M). *P<0.05, **P<0.01, ***P<0.001. Scale bars, 50 µm (B), 100 µm (A, H, K), 500 µm (F). See also Figures S1 and S2.

Figure 2: inhibiting SMAD1/5 activity in mouse cortical progenitors causes premature neurogenesis, and depletion of the RGC and IPC pools.

(A) Timeline of cortical neurogenesis and BrdU injections during mouse embryonic development. (B-J) Immunostaining and quantification of the mean numbers ± s.d. of PAX6+;TBR2- RGCs and TBR2+ IPCs (B-D), the neuronal output (% of $BrdU^+$; $Tuj1^+/BrdU^+$ cells, E, F), the generation of early-born $TBR1^+$ (G, H) and late-born $SATB2^+$ (I, J) cortical excitatory neurons quantified per radial unit (100 µm) in the developing cerebral cortex of SmadNes mutant mice and their control littermates at early (E11.5), middle (E13.5) and late (E17.5) embryonic stages, obtained from 3-5 embryos per genotype and stage. The normality was tested using the values of individual sections. Significance was assessed with the two-sided unpaired t-test (C, D, F, H, J). *P<0.05, **P<0.01, ***P<0.01. Scale bars, 50 µm. CP: cortical plate, IZ: intermediate zone, SVZ: sub-ventricular zone, VZ: ventricular zone. See also Figures S3 and S4.

Figure 3: Inhibiting SMAD1/5 activity in chick cortical RGCs increases neurogenic divisions and causes their premature depletion and differentiation.

(A) Cortical neurogenesis in the chick, showing the main cortical progenitor subtypes and their modes of division. (B) Coronal sections from 3, 5 and 8 days-old chick embryos showing the developing $PAX6^+$ cerebral cortex, formed of $SOX2^+$ neural progenitors, differentiating HuC/D^+ and $TBR1^+$ neurons, $PAX6^+$;$TBR2^-$ RGCs undergoing mitosis at the apical surface (black arrowheads) and $TBR2^+$ IPCs dividing mostly basally (white arrowheads). (C) The active, phosphorylated form of SMAD1/5/8 (pSMAD1/5/8) immunoreactivity at E5, and (D) its mean intensity ± s.d. measured in 276 apical and 93 basal mitoses obtained from 5 embryos. (E) The pSMAD1/5/8

immunoreactivity in mitotic cortical progenitors 24 hours after in ovo electroporation (IOE) with the pTis21:RFP reporter along with a control H2B-GFP-producing plasmid, and (F) its mean intensity ± s.d quantified in 137 pTis21:RFP+ neurogenic divisions and 107 pTis21:RFP- self-amplifying divisions derived from 8 electroporated embryos. (G, H) The mean proportion ± s.d. of electroporated (H2B-GFP+) cortical progenitors undergoing neurogenic pTis21:RFP+ divisions (white arrowheads) after IOE of shRNA plasmids targeting cSmad1 or cSmad5 (sh-S1/5) or their control, obtained from 9-12 embryos per experimental condition. (I) Representative images and (J) mean proportions ± s.e.m of SOX2+/-;HuC/D+/- (top), PAX6+/-;TBR2+/- (middle) and HuC/D+/-;TBR1+/- (bottom) cells among electroporated (H2B-GFP+) cells, assessed 48 hours after IOE with sh-S1, sh-S5 or their control and obtained from 5-13 embryos per experimental condition. (K) The mean proportion ± s.d of PAX6+;TBR2- RGCs (top), TBR2+ committed cells (middle) and HuC/D+ neurons (bottom) among electroporated (H2B-GFP+) cells were assessed 24 (E4), 48 (E5) and 72 (E6) hours after IOE and obtained from 6-20 embryos per condition and stage. Significance was assessed with the non-parametric Mann–Whitney test (C, D), the two-sided unpaired t-test (E) or a two-way ANOVA + Sidak's test (G, H). *P<0.05, **P<0.01, ***P<0.001. Scale bars: 50 µm (B, C, F), 10 µm (D, E). VZ: ventricular zone, MZ: mantle zone. See also Figures S5 and S6.

Figure 4: Increasing SMAD1/5 activity in chick cortical RGCs impedes neurogenic divisions and restrains differentiation.

(A) Representative images and (B) mean proportion ± s.d of electroporated (H2B-GFP+) cortical progenitors undergoing neurogenic pTis21:RFP+ divisions (white arrowheads) after IOE of a constitutively active SMAD5 mutant (5-S/D) or its control,

obtained from 8-9 embryos per experimental condition. (C) Representative images and (D) mean proportion ± s.e.m of PAX6+/-;TBR2+/- and SOX2+/-;HuC/D+/- cells among electroporated (H2B-GFP+) cells 48 hours after IOE of 5-S/D or its control, obtained from 7-15 embryos per experimental condition. (E) Representative images and (F) mean proportion ± s.e.m of SOX2+/-;HuC/D+/- cells among electroporated (H2B-GFP+) cells 48 hours after IOE of a control plasmid, or sh-S5 combined with a control plasmid (sh-S5) or with the constitutively active SMAD5-S/D mutant (sh-S5+5-S/D), obtained from 8-13 embryos per condition. Significance was assessed with the two-sided unpaired t-test (B), a two-way ANOVA + Sidak's (D) or + Tukey's (F) tests. **P<0.01; ***P<0.001. Scale bars: 10 µm (A), 50 µm (C, E). See also Figures S7.

Figure 5: Transcriptional program regulated by SMAD1/5 in early mouse cortical RGCs.

(A) Methodology used to compare the transcriptome of cortical RGCs from SmadNes mutant and control E12.5 embryos. (B) Spearman rank correlation and heatmap representing the differentially expressed transcripts (DETs, with a pAdj<0.05) between mutant and control cortical RGCs. (C, D) Representation of the top 10 gene ontology biological processes (C) and transcription factor binding motifs (D) associated with the DETs (with a pAdj<0.1). See also Tables S1 and S2.

Figure 6: SMAD1/5 regulate early cortical neurogenesis through YAP.

(A) Upon BMP activity, SMAD1/5 are activated and can physically interact and act synergistically with YAP. When SMAD1/5 activity is reduced or abrogated, YAP is inactivated and primed for proteosomal degradation. (B) Expression of YAP during early mouse corticogenesis (E11.5), relative to SMAD1/5 activity (pSMAD1/5/8). The

mean intensity ± s.d. of endogenous YAP (C) and pSMAD1/5/8 (D) immunoreactivity was quantified in 70 apical and 28 basal pH3+ mitotic nuclei, obtained from 3 embryos and (E) the correlation between their intensities assessed by the Pearson's correlation coefficient r. (F) Immunostaining of the developing chick cerebral cortex for total YAP 24 hours after IOE with a control or sh-S1/5 plasmid and (G) its mean ratio ± s.d. quantified in electroporated relative to non-electroporated mitotic cells obtained from 7 embryos (Ctrl: 147 pH3+;GFP+ cells and 154 pH3+;GFP- cells, sh-S1/5: 162 pH3+;GFP+ cells and 140 pH3+;GFP- cells). (H) Immunostaining of pYAP and total YAP and (I) quantification of the pYAP/YAP intensity ratio ± s.d. in the developing cerebral cortex of E11.5 SmadNes mutant embryos and control littermates, obtained from 4 embryos (12 sections) per genotype. The normality was tested using the values of individual sections. (J-N) Immunostaining (J) and mean proportion ± s.e.m (K-N) of SOX2+/-;HuC/D+/- cells (K), RGCs (PAX6+;TBR2- cells, L), TBR2+ cells (M) and ectopic SOX2+ cells (N) among electroporated (GFP+) cells 48 hours after IOE of a wild type YAP1 construct (YAP) together with sh-S1 or its control, obtained from n=8-9 embryos per condition. (O) Model proposing that upon BMP signalling, the activated SMAD1/5 recruit YAP to promote RGC self-amplification. When SMAD1/5 activity is reduced or abrogated and YAP is inactivated and primed for degradation, their transcriptional activity is suppressed, thereby enabling RGCs to undergo neurogenic divisions. Significance was assessed with the non-parametric Mann–Whitney test (C, D, G), the two-sided unpaired t-test (I) or a two-way ANOVA + Tukey's multiple comparisons test (K-N). *P<0.05, **P<0.01, ***P<0.001. Scale bars, 50 µm. See also Figure S8.

Materials and Methods

Animals

Smad1$^{wt/fl}$;Smad5$^{wt/fl}$;Nestin:Cre$^{+/0}$ embryos and postnatal mice were obtained by crossing *Smad1$^{fl/fl}$;Smad5$^{fl/fl}$* mice with transgenic mice that express Cre-recombinase in neural progenitor cells and somites from E8.5 (*NesCre8* mice: (Moya et al., 2012; Petersen et al., 2002). Smad1$^{wt/fl}$;Smad5$^{wt/fl}$;Nestin:Cre$^{0/0}$ littermates were used as controls. The days of the vaginal plug and birth were defined as E0.5 and P0, respectively. *Smad1$^{fl/fl}$;Smad5$^{fl/fl}$* and *NesCre8* mice were maintained in their original genetic backgrounds. All the experimental procedures were carried out in accordance with the European Union guidelines (Directive 2010/63/EU) and the followed protocols were approved by the ethics committee of the Parc Científic de Barcelona (PCB).

Fertilized white Leghorn chicken eggs were provided by Granja Gibert, rambla Regueral, S/N, 43850 Cambrils, Spain. Eggs were incubated in a humidified atmosphere at 38°C in a Javier Masalles 240N incubator for the appropriate duration and staged according to the method of Hamburger and Hamilton (HH: (Hamburger and Hamilton, 1951). According to EU animal care guidelines, no IACUC approval was necessary to perform the experiments described herein, considering that the embryos used in this study were always harvested at early stages of embryonic development. Sex was not identified at these stages.

In ovo electroporation

Unilateral *in ovo* electroporations were performed in the developing chick dorsal telencephalon at stage HH18 (E3, 69-72 hours of incubation). Analyses were performed specifically in the dorsal-medial-lateral region of the developing chick cerebral cortex to minimize any possible variability along the medial-lateral axis. Plasmids were diluted in

RNAse-free water at the required concentration [0 to 4 µg/µl] and injected into the right cerebral ventricle using a fine glass needle. Electroporation was triggered by applying 5 pulses of 50 ms at 22.5 V with 50 ms intervals using an Intracel Dual Pulse (TSS10) electroporator. Electroporated chicken embryos were incubated back at 38°C and recovered at the times indicated.

Plasmids

Inhibition of *cSmad1* and *cSmad5* expression was triggered by electroporation of short-hairpin constructs inserted into the pSuper (Oligoengine) or pSHIN vectors together with a control H2B-GFP-producing plasmid as previously reported (Kojima et al., 2004; Le Dreau et al., 2018; Le Dreau et al., 2012). Electroporation of 2-4 µg/µl of these constructs caused a specific and reproducible 50% inhibition of the target expression (Le Dreau et al., 2012). The pCAGGS_SMAD5-SD_ires_GFP, its control pCAGGS_ires_GFP (pCIG), as well as the pTis21:RFP reporter used to assess the modes of divisions undergone by spinal progenitors, were previously described in details (Le Dreau et al., 2012; Megason and McMahon, 2002; Saade et al., 2013). The pCAGGS_Flag-YAP1_ires_GFP construct was obtained by subcloning from a pCDNA:Flag-YAP1 kindly provided by Conchi Estaras (Levy et al., 2008).

In situ hybridization

Chicken embryos were recovered at the indicated stages, fixed overnight at 4 ºC in 4% paraformaldehyde (PFA), rinsed in PBS and processed for whole mount RNA *in situ* hybridization following standard procedures. Probes against chick *Smad1* (#chEST899n18) and *Smad8* (#chEST222h17) were purchased from the chicken EST project (UK-HGMP RC). Probe against *cSmad5* was kindly provided by Dr Marian

Ros. Hybridized embryos were post-fixed in 4% PFA and washed in PBT, and 45 µM-thick vibratome sections (VT1000S, Leica) were mounted and photographed under a microscope (DC300, Leica). The data show representative images obtained from 3 embryos for each stage and probe. The images of *mSmad1, mSmad5 and mSmad8* expression in the developing mouse dorsal telencephalon at E14.5 were obtained from the Genepaint database (https://gp3.mpg.de).

Histology and Immunohistochemistry

Mouse embryos were recovered at the indicated stages and their heads fixed by immersion in 4% PFA for 24 hours at 4 ºC, cryoprotected with 30% sucrose in PBS, embedded in Tissue-Tek O.C.T. (Sakura Finetek), frozen in isopentane at -30 ºC and sectioned coronally on a cryostat (Leica). Cryosections (14 µm) were collected on Starfrost pre-coated slides (Knittel Glasser) and distributed serially. Postnatal and adult mice were deeply anesthetized in a CO_2 chamber and trans-cardially perfused with 4% PFA. The brains were removed, post-fixed and cryoprotected as indicated above and cryotome (40 µm) sections were then distributed serially. Chicken embryos were carefully dissected, fixed for 2 hours at room temperature (RT) in 4% PFA, rinsed in PBS and cryoprotected with 30% sucrose in PBS and 16 µm-thick coronal sections prepared with a cryostat.

For both species, immunostaining was performed following standard procedures. After washing in PBS containing 0.1% Triton X-100 (PBT), the sections were blocked for 1 hour at RT in PBT supplemented with 10% bovine serum albumin (BSA). When necessary, sections were submitted to an antigen retrieval treatment before blocking by boiling sections for 10 min in sodium citrate buffer (2 mM citric acid monohydrate, 8 mM tri-sodium citrate dihydrate, pH 6.0). For BrdU immunostaining, sections were

incubated before blocking in 50% formamide in 2X SSC at 64 ºC for 10 min followed by an incubation in 2N HCl at 37 ºC for 30 min and finally 10 min in 0.1 M boric acid (pH 8.5) at RT. Sections were then incubated overnight at 4 ºC with the appropriate primary antibodies (Table S2) diluted in a solution of PBT supplemented with 10% BSA or sheep serum. After washing in PBT, sections were incubated for 2 hours at RT with the appropriate secondary antibodies diluted in PBT supplemented with 10% BSA or sheep serum. Alexa488-, Alexa555- and Cy5-conjugated secondary antibodies were obtained from Invitrogen and Jackson Laboratories. Sections were finally stained with 1 µg/ml DAPI and mounted in Mowiol (Sigma-Aldrich).

Cell cycle exit assay

Pregnant female mice received an intra-peritoneal injection of BrdU (100 mg/kg; Sigma) and were sacrificed 24 hours later. Embryos were collected and processed as described above. Sections were immunostained for BrdU and Tuj1 and the cell cycle exit rate (neuronal output) was estimated by quantifying the proportion of $BrdU^+$-immunolabelled cells that were $Tuj1^+$ (% of $Tuj1^+$;$BrdU^+$/$BrdU^+$ cells).

Image acquisition and treatment

Optical sections of mouse and chick embryo fixed samples (coronal views) were acquired at RT with the Leica LAS software, in a Leica SP5 confocal microscope using 10x (dry HC PL APO, NA 0.40), 20x (dry HC PL APO, NA 0.70), 40x (oil HCX PL APO, NA 1.25-0.75) or 63x (oil HCX PL APO, NA 1.40-0.60) objective lenses. Maximal projections obtained from 2µm Z-stack images were processed in Photoshop CS5 (Adobe) or ImageJ for image merging, resizing and cell counting. Optical sections of postnatal and adult mouse samples were acquired with a Leica AF7000 motorized

wide-field microscope. Cell counting in embryo, postnatal and adult mouse samples were performed in a 100 or 200 μm-wide radial column of the lateral cortical wall, as indicated in the figures. Cell counts were performed in a minimum of 3 sections of the same rostral-caudal level per embryo or postnatal mouse sample. Cell counting and measurements of the layers' thickness in the P7 and P60 mouse cerebral cortex was done based on DAPI staining combined to MEFC2/SATB2 and NeuN immunostaining, respectively. Quantification of pSMAD1/5/8, PAX6, TBR2, YAP and pYAP intensities was assessed using the ImageJ software. Cell nuclei of mitotic $pH3^+$ cells or $H2B\text{-}GFP^+$ electroporated and neighboring non-electroporated cells were delimitated by polygonal selection, and the mean intensity was quantified as mean gray values.

Western blot

Total protein extracts (≈ 40 μg) were resolved by SDS-PAGE following standard procedures and transferred onto a nitrocellulose membrane (Hybond-ECL, Amersham Biosciences) that was probed with the primary antibodies (Table S2) whose binding was detected by infra-red fluorescence using the LI-COR Odyssey IR Imaging System V3.0 (LI-COR Biosciences).

Purification of mouse Prominin1$^+$ RGCs

The purification of Prominin1$^+$ cortical RGCs was achieved by fluorescence-activated cell sorting (FACS) of dissociated cells obtained from the forebrain of Smad1$^{wt/fl}$;Smad5$^{wt/fl}$;Nestin:Cre$^{+/0}$ and Smad1$^{wt/fl}$;Smad5$^{wt/fl}$;Nestin:Cre$^{0/0}$ E12.5 embryos. Forebrains of littermates with the same genotype were pooled and incubated in Hanks' balanced salt solution (HBSS) containing 0.6% Glucose and 5 mM EDTA for 5 min at 37 ºC. Cells were mechanically dissociated by gentle trituration and collected

by centrifugation at 300 g for 10 min at 4 ºC. Cells were resuspended in 200 µl of incubation media (PBS containing 0.6% glucose, 2% foetal bovine serum and 0.02% NaN_3) and kept for 10 min at 4 ºC with mild agitation. Cells were then incubated for 30 min at 4 ºC with an APC-conjugated anti-Prominin1 antibody (eBioscience, #17-1331-81) diluted at 0.2 mg/ml. Incubation with a rat IgG1-APC antibody was performed in parallel to define non-specific fluorescence. After the incubation, cells were centrifuged at 300 g for 10 min at 4 ºC and incubated with 1 ml of incubation media. Dissociated cells were then filtered through a falcon tube with a cell strainer cap (BD Biosciences; BD falcon 12 x 75 mm) in which the filter was previously dampened with 500 µl of incubation media. The number of isolated cells was determined using a Neubauer chamber and cells were diluted to a final concentration of 2-3 x 10^6 cells/ml. DAPI (20 ng/mL: Vector Labs) was added to identify dead cells. Sorting was performed with a BD FACS Aria™ Fusion (BD Biosciences) cytometer. After sorting, collector tubes were centrifuged at 1000 g for 10 min at 4 ºC and cell pellets stored at -80 ºC.

RNA-sequencing

RNA was extracted from pools of 6 x 10^5 FACS-isolated cells using the miRNeasy Micro Kit (Qiagen). Quantification of total RNA was performed by Qubit® RNA BR Assay kit (Thermo Fisher Scientific) and RNA 6000 Nano Bioanalyzer 2100 Assay (Agilent) was used to estimate the total RNA integrity. The 3 pairs of samples of RNAs from SmadNes mutant and control RGCs presenting the best RNA integrity were used for sequencing. Sample preparation protocol for the RNASeq libraries was following the manufacturer's recommendations of KAPA Stranded mRNA-Seq Illumina® Platforms Kit (Roche-Kapa Biosystems). The libraries were sequenced on HiSeq2500 (Illumina) in paired-end mode with a read length of 2 x 100 bp using TruSeq SBS Kit

v4 (Illumina). Each sample was sequenced in a fraction of a sequencing v4 flow cell lane, following the manufacturer's protocol. Image analysis, base calling and quality scoring of the run were processed using the manufacturer's software Real Time Analysis (RTA 1.18.66.3) and followed by generation of FASTQ sequence files.

RNA-Seq paired-end reads were mapping against *Mus musculus* reference genome (GRCm38) using STAR version 2.5.3a (Dobin et al., 2013) with ENCODE parameters for long RNA. Isoforms were quantified using RSEM version 1.3.0 (Li and Dewey, 2011) with default parameters for stranded sequencing and the gencode version M15. Differential isoform analysis was performed with DESeq2 version 1.18 (Love et al., 2014) with default parameters. We considered differentially expressed transcripts those showing a *p*-adjusted value < 0.05 or *p*-adjusted value <0.1 (extended list). Fold-change (FC) values between genotypes (SmadNes mutants over controls) are expressed in Log2 (Table S1). The GO term enrichment analysis (biologic process) of the extended DET signature was performed with the PANTHER classification system (http://pantherdb.org) and the Transfac/Jaspar analysis using Enrichr (Chen et al., 2013; Kuleshov et al., 2016).

Statistical analyses

No statistical method was used to predetermine sample size. The experiments were not randomized. The investigators were not blinded to allocation during experiments. Statistical analyses were performed using the GraphPad Prism 6 software (GraphPad Software, Inc.). Unless noted otherwise (see quantifications), cell counts were typically performed on 3-5 images per embryo and *n* values correspond to different embryos or animals. The normal distribution of the values was assessed by the Shapiro-Wilk normality test. Significance was then assessed with a two-sided

unpaired t-test, one-way ANOVA + Tukey's test or two-way ANOVA + Sidak's or Tukey's test for data presenting a normal distribution, or alternatively with the non-parametric Mann–Whitney test for non-normally distributed data. The following convention was used: n.s, non-significant; *P<0.05, **P<0.01, ***P<0.001. The detailed information related to quantifications are detailed in the figure legends.

Supplemental items

Figure S1: Reduction in SMAD1/5 protein levels in the SmadNes heterozygous mutant mice.

Figure S2: The SmadNes heterozygous mutant mice present microcephaly.

Figure S3: Absence of patterning defects in the cerebral cortex of SmadNes mutant embryos.

Figure S4: The mitotic index of RGCs and IPCs is not altered in the cerebral cortex of SmadNes mutant embryos.

Figure S5: Expression of cSmad1/5/8 during chick cortical neurogenesis.

Figure S6: The activity of the pTis21:RFP reporter identifies neurogenic divisions during early chick cortical neurogenesis.

Figure S7: Increasing SMAD5 activity causes the abnormal generation of ectopic rosettes of cortical progenitors.

Figure S8: SMAD1/5 regulate early cortical neurogenesis through YAP.

Table S1: List of differentially expressed transcripts between cortical RGCs from SmadNes mutant and control E12.5 embryos.

Table S2: Expression of the genes of the Hippo signalling pathway in cortical RGCs from SmadNes mutant and control E12.5 embryos.

Table S3: List of primary antibodies used in this study.

Figures

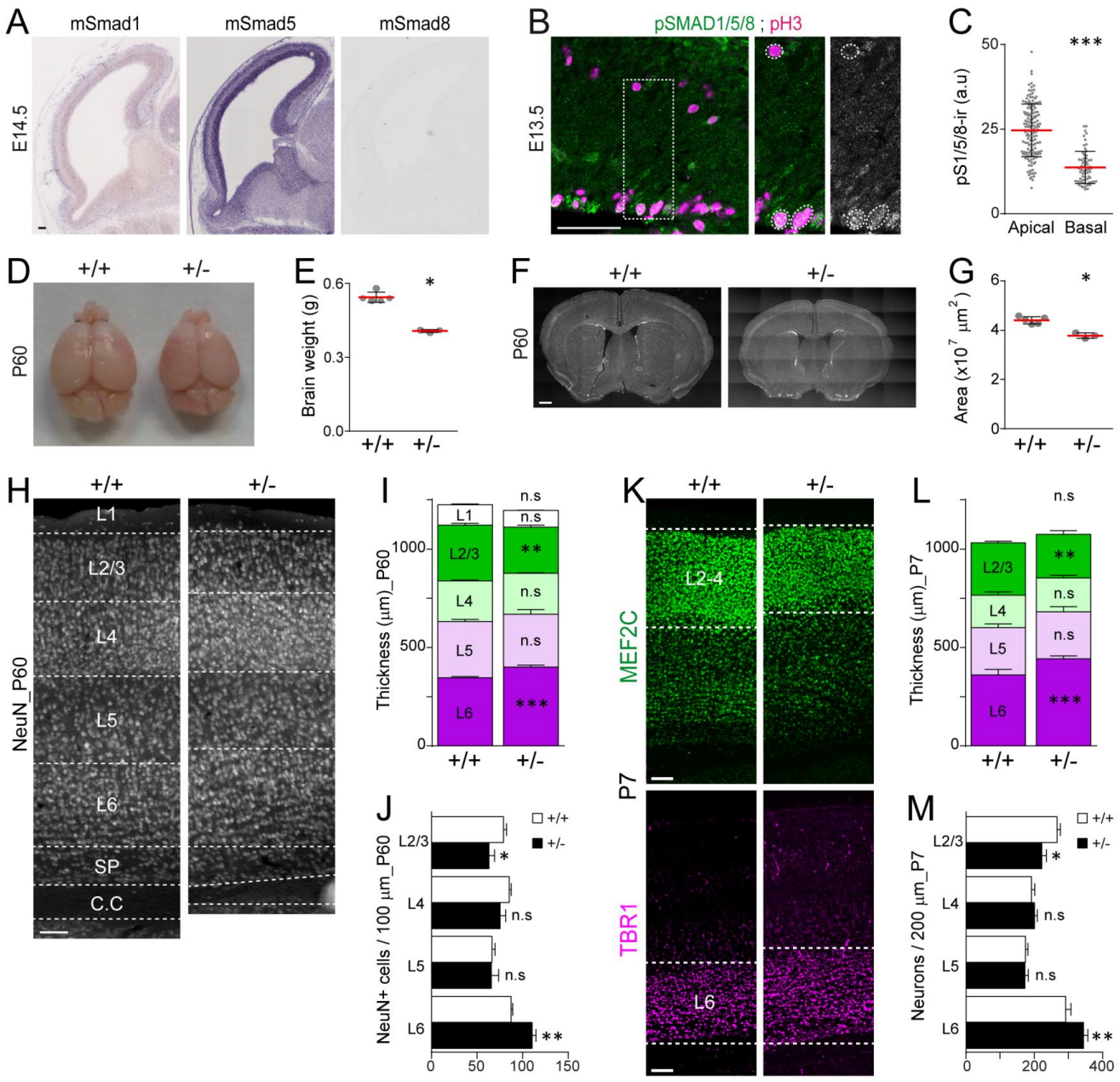
A
mSmad1
mSmad5
mSmad8
E14.5
B
pSMAD1/5/8 ; pH3
E13.5
C
pS1/5/8-ir (a.u)
Apical
Basal
D
+/+
+/-
P60
E
Brain weight (g)
F
G
Area (x10^7 µm^2)
H
NeuN_P60
L1
L2/3
L4
L5
L6
SP
C.C
I
Thickness (µm)_P60
n.s
J
NeuN+ cells / 100 µm_P60
K
MEF2C
L2-4
P7
TBR1
L
Thickness (µm)_P7
M
Neurons / 200 µm_P7

Figure 1

Figure 1: inhibiting SMAD1/5 activity in mouse neural progenitors causes microcephaly and alters the numbers of early- and late-born neocortical neurons.

(A) Sagittal sections of the developing mouse dorsal telencephalon showing mSmad1, mSmad5 and mSmad8 transcripts at E14.5, obtained from Genepaint (https://gp3.mpg.de). (B) The pSMAD1/5/8 immunoreactivity at E13.5 and (C) its mean intensity ± s.d. measured in 144 apical and 64 basal mitoses obtained from 3 mouse E13.5 embryos. (D) Images, (E) mean weight ± s.d, (F) coronal sections of the brains of SmadNes mutant mice (+/-) and their control littermates (+/+) and (G) their surface area ± s.d at P60, obtained from 3-5 animals per genotype. (H) Neuronal layer organization, (I) mean thickness of the layers ± s.e.m and (J) mean number of neurons ± s.e.m in the different layers in radial units (100 µm) of the cerebral cortex of SmadNes mutant mice and their control littermates at P60, obtained from 3-4 animals per genotype. (K) Representative images of early-born $TBR1^+$ L6 and late-born $MEF2C^+$ L4-2/3 projection neurons, (L) mean thickness of the layers ± s.e.m and (M) mean number of neurons ± s.e.m in the different layers in radial units (200 µm) of the developing cerebral cortex of the SmadNes mutant pups and their control littermates at P7, obtained from 5-6 animals per genotype. Significance was assessed with the non-parametric Mann–Whitney test (C, E, G; I and L for the total cumulated thickness) or a two-way ANOVA + Sidak's test (I, J, L, M). *P<0.05, **P<0.01, ***P<0.001. Scale bars, 50 µm (B), 100 µm (A, H, K), 500 µm (F). See also Figures S1 and S2.

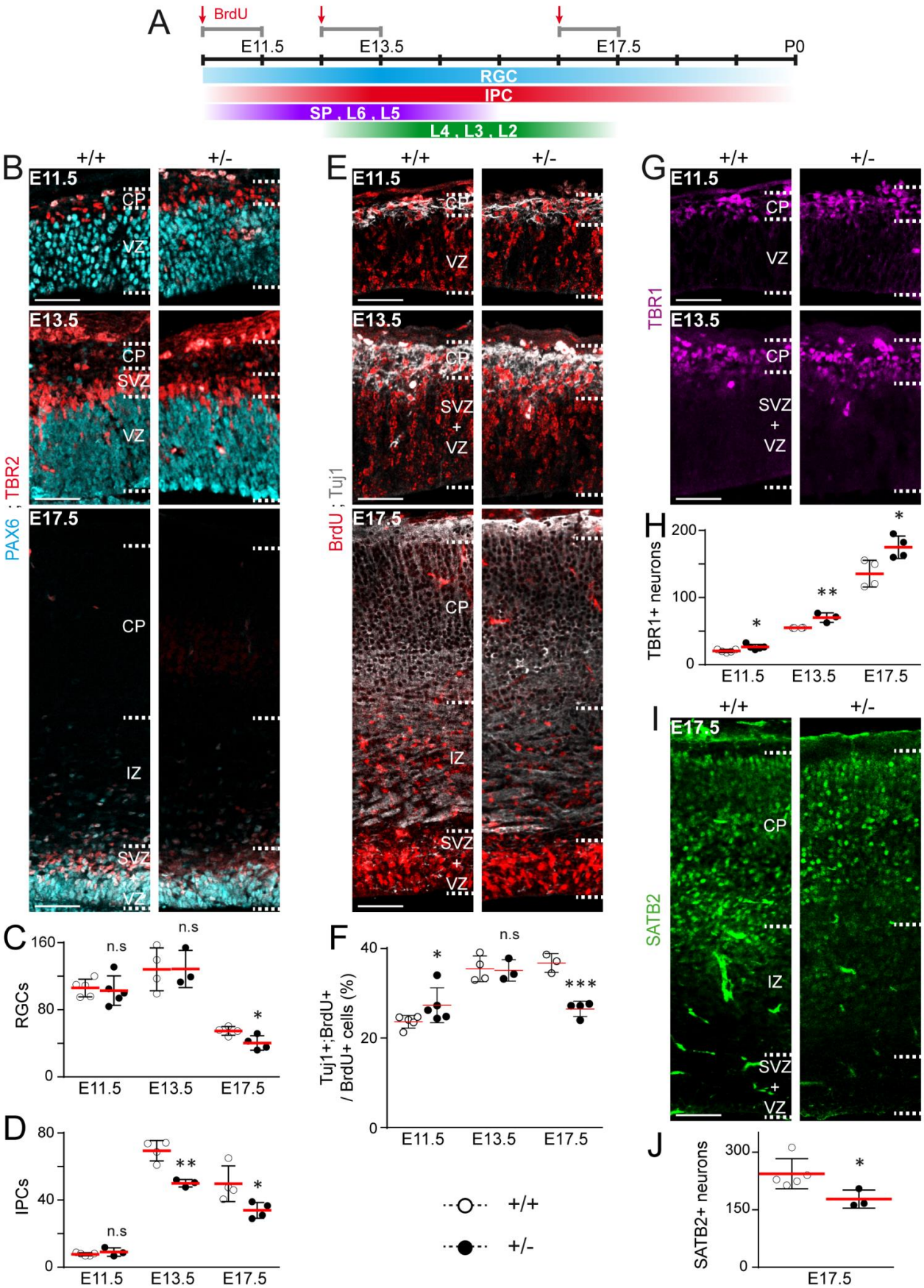
A
BrdU
E11.5
E13.5
E17.5
P0
RGC
IPC
SP , L6 , L5
L4 , L3 , L2
B
+/+
+/-
E11.5
E13.5
E17.5
CP
VZ
SVZ
IZ
PAX6 ; TBR2
C
RGCs
n.s
D
IPCs
E
BrdU ; Tuj1
F
Tuj1+;BrdU+ / BrdU+ cells (%)
G
TBR1
H
TBR1+ neurons
I
SATB2
J
SATB2+ neurons

Figure 2

Figure 2: inhibiting SMAD1/5 activity in mouse cortical progenitors causes premature neurogenesis, and depletion of the RGC and IPC pools.

(A) Timeline of cortical neurogenesis and BrdU injections during mouse embryonic development. (B-J) Immunostaining and quantification of the mean numbers ± s.d. of PAX6+;TBR2- RGCs and TBR2+ IPCs (B-D), the neuronal output (% of $BrdU^+$; $Tuj1^+/BrdU^+$ cells, E, F), the generation of early-born $TBR1^+$ (G, H) and late-born $SATB2^+$ (I, J) cortical excitatory neurons quantified per radial unit (100 µm) in the developing cerebral cortex of SmadNes mutant mice and their control littermates at early (E11.5), middle (E13.5) and late (E17.5) embryonic stages, obtained from 3-5 embryos per genotype and stage. The normality was tested using the values of individual sections. Significance was assessed with the two-sided unpaired t-test (C, D, F, H, J). *P<0.05, **P<0.01, ***P<0.01. Scale bars, 50 µm. CP: cortical plate, IZ: intermediate zone, SVZ: sub-ventricular zone, VZ: ventricular zone. See also Figures S3 and S4.

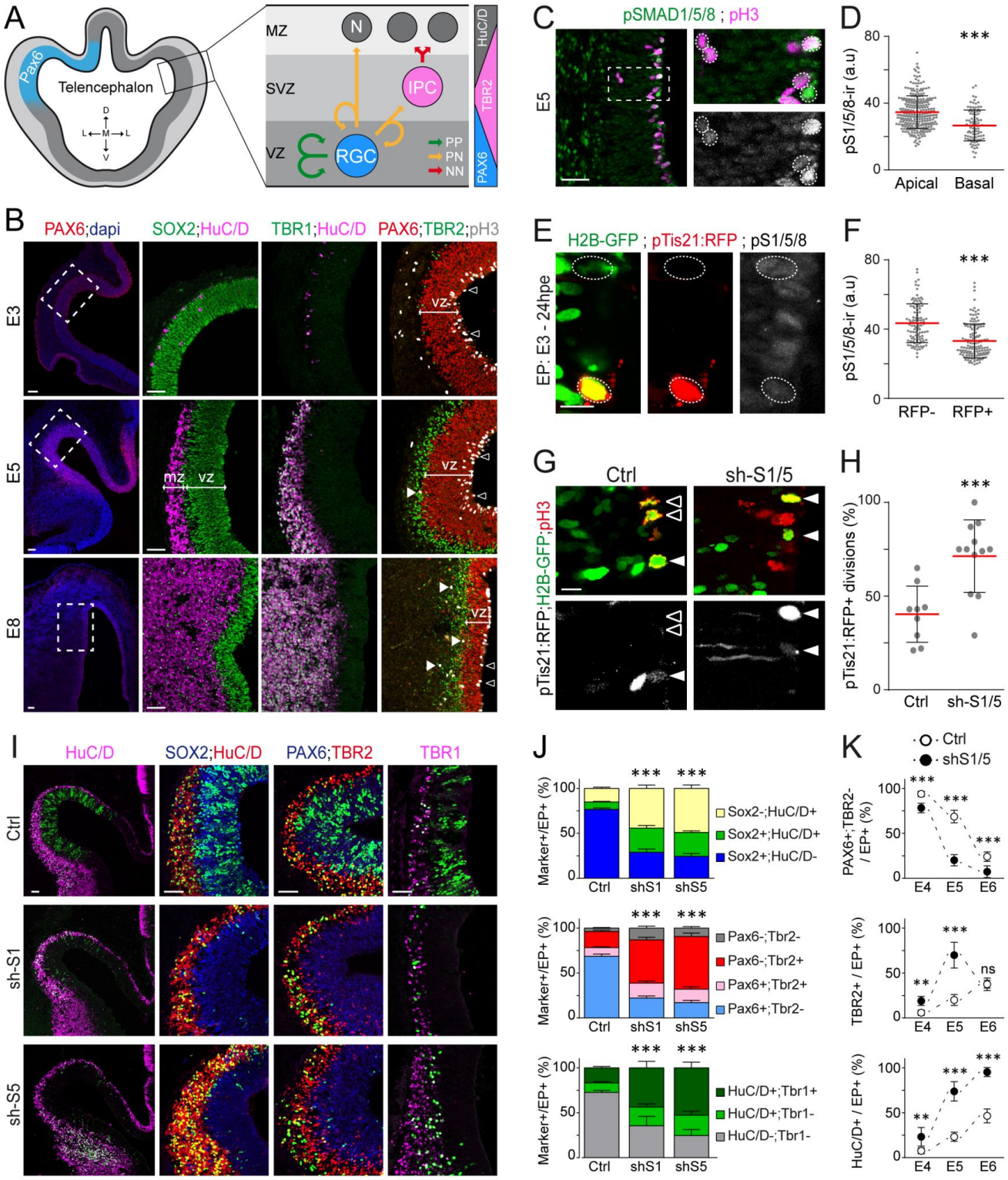
A
Pax6
Telencephalon
D
L
M
L
V
MZ
SVZ
VZ
N
IPC
RGC
PP
PN
NN
HuC/D
TBR2
PAX6
B
PAX6;dapi
SOX2;HuC/D
TBR1;HuC/D
PAX6;TBR2;pH3
E3
E5
E8
mz
vz
C
pSMAD1/5/8 ; pH3
E5
D
pS1/5/8-ir (a.u)
Apical
Basal
E
H2B-GFP ; pTis21:RFP ; pS1/5/8
EP: E3 - 24hpe
F
RFP-
RFP+
G
Ctrl
sh-S1/5
pTis21:RFP;H2B-GFP;pH3
H
pTis21:RFP+ divisions (%)
I
HuC/D
SOX2;HuC/D
PAX6;TBR2
TBR1
Ctrl
sh-S1
sh-S5
J
Marker+/EP+ (%)
Sox2-;HuC/D+
Sox2+;HuC/D+
Sox2+;HuC/D-
Pax6-;Tbr2-
Pax6-;Tbr2+
Pax6+;Tbr2+
Pax6+;Tbr2-
HuC/D+;Tbr1+
HuC/D+;Tbr1-
HuC/D-;Tbr1-
shS1
shS5
K
Ctrl
shS1/5
PAX6+;TBR2- / EP+ (%)
TBR2+ / EP+ (%)
HuC/D+ / EP+ (%)
E4
E5
E6
ns

Figure 3

Figure 3: Inhibiting SMAD1/5 activity in chick cortical RGCs increases neurogenic divisions and causes their premature depletion and differentiation.

(A) Cortical neurogenesis in the chick, showing the main cortical progenitor subtypes and their modes of division. (B) Coronal sections from 3, 5 and 8 days-old chick embryos showing the developing $PAX6^+$ cerebral cortex, formed of $SOX2^+$ neural progenitors, differentiating HuC/D^+ and $TBR1^+$ neurons, $PAX6^+$;$TBR2^-$ RGCs undergoing mitosis at the apical surface (black arrowheads) and $TBR2^+$ IPCs dividing mostly basally (white arrowheads). (C) The active, phosphorylated form of SMAD1/5/8 (pSMAD1/5/8) immunoreactivity at E5, and (D) its mean intensity ± s.d. measured in 276 apical and 93 basal mitoses obtained from 5 embryos. (E) The pSMAD1/5/8 immunoreactivity in mitotic cortical progenitors 24 hours after in ovo electroporation (IOE) with the pTis21:RFP reporter along with a control H2B-GFP-producing plasmid, and (F) its mean intensity ± s.d quantified in 137 pTis21:RFP+ neurogenic divisions and 107 pTis21:RFP- self-amplifying divisions derived from 8 electroporated embryos. (G, H) The mean proportion ± s.d. of electroporated (H2B-GFP+) cortical progenitors undergoing neurogenic pTis21:RFP+ divisions (white arrowheads) after IOE of shRNA plasmids targeting cSmad1 or cSmad5 (sh-S1/5) or their control, obtained from 9-12 embryos per experimental condition. (I) Representative images and (J) mean proportions ± s.e.m of SOX2+/-;HuC/D+/- (top), PAX6+/-;TBR2+/- (middle) and HuC/D+/-;TBR1+/- (bottom) cells among electroporated (H2B-GFP+) cells, assessed 48 hours after IOE with sh-S1, sh-S5 or their control and obtained from 5-13 embryos per experimental condition. (K) The mean proportion ± s.d of PAX6+;TBR2- RGCs (top), TBR2+ committed cells (middle) and HuC/D+ neurons (bottom) among electroporated (H2B-GFP+) cells were assessed 24 (E4), 48 (E5) and 72 (E6) hours after IOE and obtained from 6-20 embryos per condition and stage. Significance was assessed with the non-parametric Mann–Whitney test (C, D), the two-sided unpaired t-test (E) or a two-way ANOVA + Sidak's test (G, H). *P<0.05, **P<0.01, ***P<0.001. Scale bars: 50 µm (B, C, F), 10 µm (D, E). VZ: ventricular zone, MZ: mantle zone. See also Figures S5 and S6.

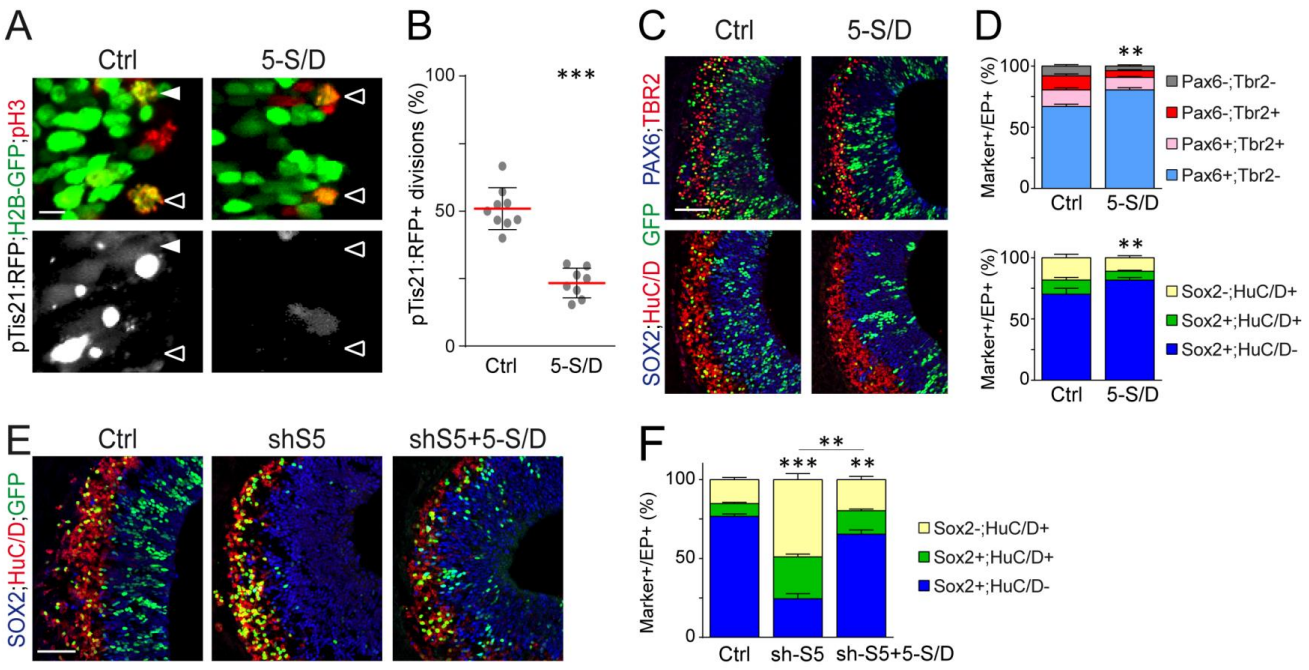
A
Ctrl
5-S/D
pTis21:RFP;H2B-GFP;pH3
B
pTis21:RFP+ divisions (%)
100
50
0
***
Ctrl
5-S/D
C
Ctrl
5-S/D
PAX6;TBR2
GFP
SOX2;HuC/D
D
Marker+/EP+ (%)
100
50
0
**
Pax6-;Tbr2-
Pax6-;Tbr2+
Pax6+;Tbr2+
Pax6+;Tbr2-
Ctrl
5-S/D
Sox2-;HuC/D+
Sox2+;HuC/D+
Sox2+;HuC/D-
E
Ctrl
shS5
shS5+5-S/D
SOX2;HuC/D;GFP
F
Marker+/EP+ (%)
***
**
**
Sox2-;HuC/D+
Sox2+;HuC/D+
Sox2+;HuC/D-
Ctrl
sh-S5
sh-S5+5-S/D

Figure 4

Figure 4: Increasing SMAD1/5 activity in chick cortical RGCs impedes neurogenic divisions and restrains differentiation.

(A) Representative images and (B) mean proportion ± s.d of electroporated (H2B-GFP+) cortical progenitors undergoing neurogenic pTis21:RFP+ divisions (white arrowheads) after IOE of a constitutively active SMAD5 mutant (5-S/D) or its control, obtained from 8-9 embryos per experimental condition. (C) Representative images and (D) mean proportion ± s.e.m of PAX6+/-;TBR2+/- and SOX2+/-;HuC/D+/- cells among electroporated (H2B-GFP+) cells 48 hours after IOE of 5-S/D or its control, obtained from 7-15 embryos per experimental condition. (E) Representative images and (F) mean proportion ± s.e.m of SOX2+/-;HuC/D+/- cells among electroporated (H2B-GFP+) cells 48 hours after IOE of a control plasmid, or sh-S5 combined with a control plasmid (sh-S5) or with the constitutively active SMAD5-S/D mutant (sh-S5+5-S/D), obtained from 8-13 embryos per condition. Significance was assessed with the two-sided unpaired t-test (B), a two-way ANOVA + Sidak's (D) or + Tukey's (F) tests. **P<0.01; ***P<0.001. Scale bars: 10 µm (A), 50 µm (C, E). See also Figures S7.

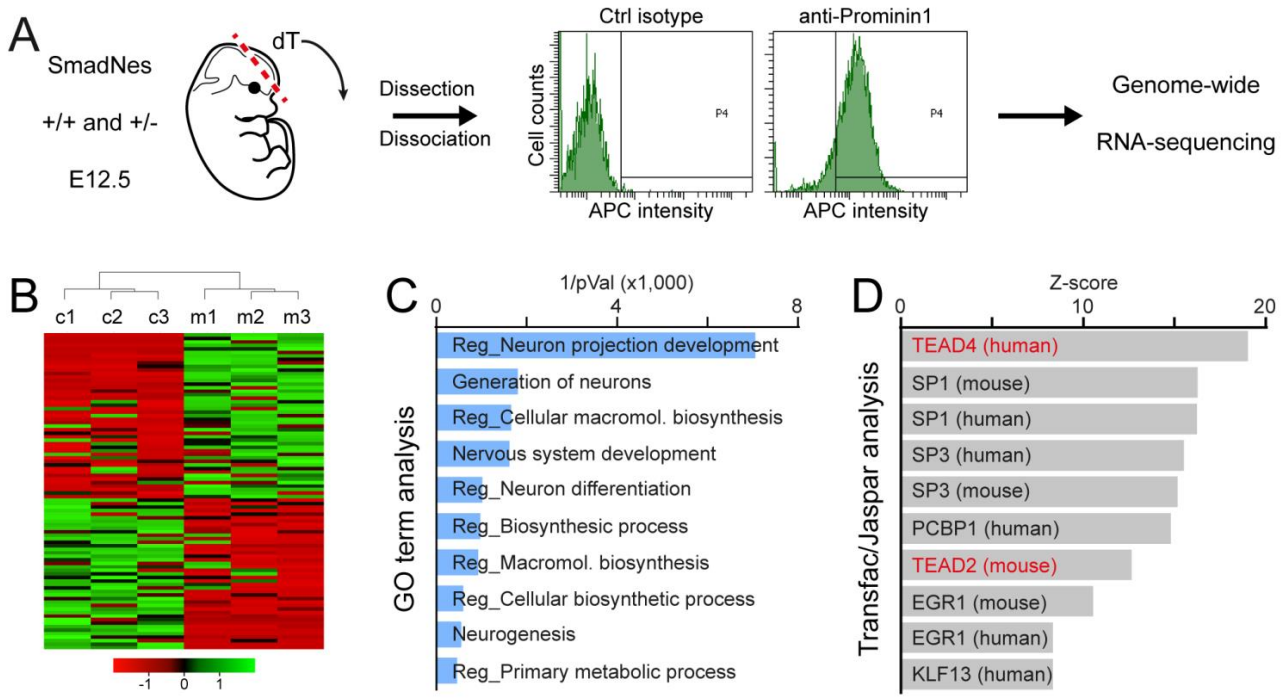
A
SmadNes
+/+ and +/-
E12.5
dT
Dissection
Dissociation
Ctrl isotype
anti-Prominin1
Cell counts
P4
APC intensity
Genome-wide
RNA-sequencing
B
c1
c2
c3
m1
m2
m3
-1
0
1
C
1/pVal (x1,000)
0
4
8
GO term analysis
Reg_Neuron projection development
Generation of neurons
Reg_Cellular macromol. biosynthesis
Nervous system development
Reg_Neuron differentiation
Reg_Biosynthesic process
Reg_Macromol. biosynthesis
Reg_Cellular biosynthetic process
Neurogenesis
Reg_Primary metabolic process
D
Z-score
0
10
20
Transfac/Jaspar analysis
TEAD4 (human)
SP1 (mouse)
SP1 (human)
SP3 (human)
SP3 (mouse)
PCBP1 (human)
TEAD2 (mouse)
EGR1 (mouse)
EGR1 (human)
KLF13 (human)

Figure 5

Figure 5: Transcriptional program regulated by SMAD1/5 in early mouse cortical RGCs.

(A) Methodology used to compare the transcriptome of cortical RGCs from SmadNes mutant and control E12.5 embryos. (B) Spearman rank correlation and heatmap representing the differentially expressed transcripts (DETs, with a pAdj<0.05) between mutant and control cortical RGCs. (C, D) Representation of the top 10 gene ontology biological processes (C) and transcription factor binding motifs (D) associated with the DETs (with a pAdj<0.1). See also Tables S1 and S2.

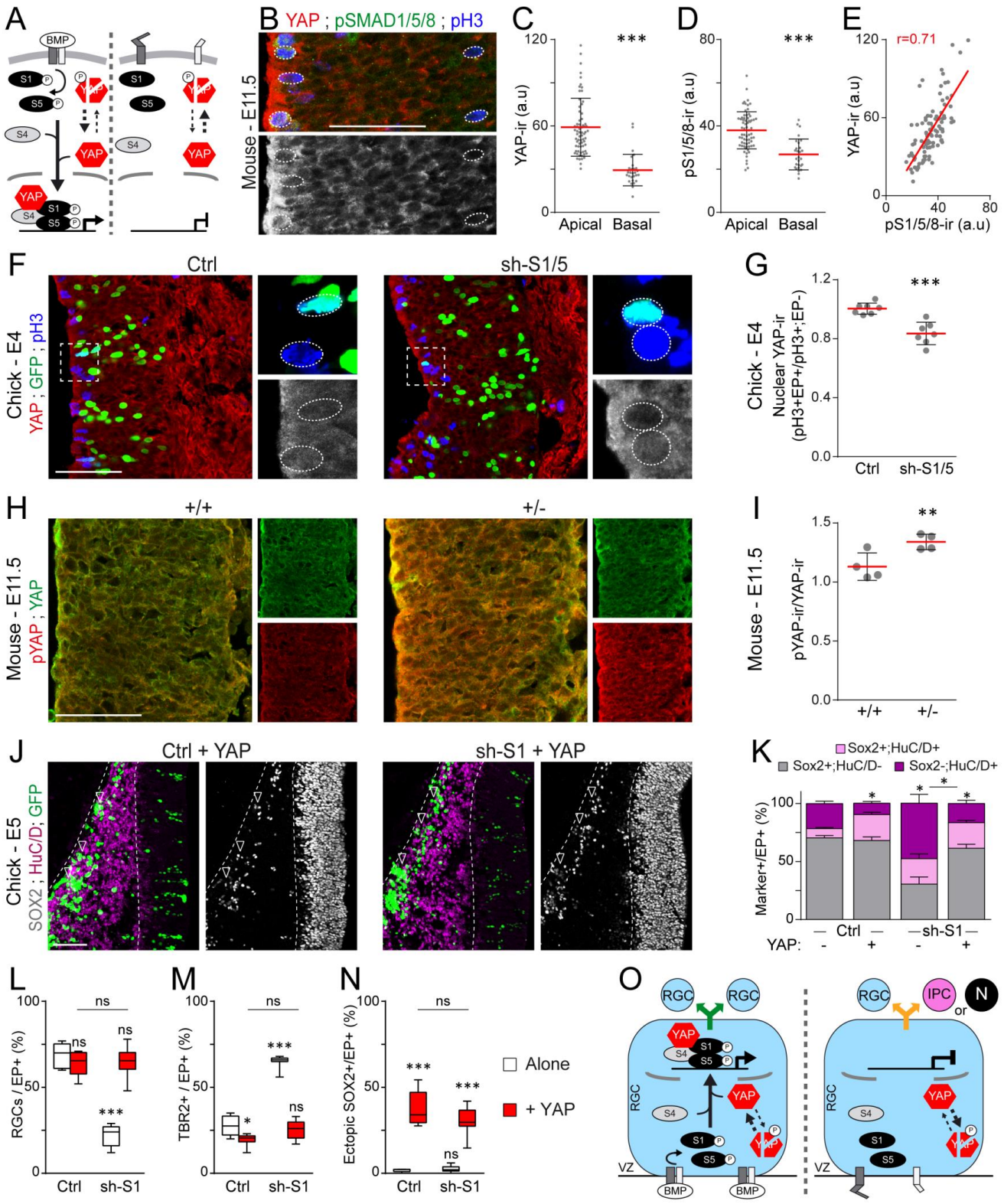
A
BMP
S1
S5
S4
YAP
B YAP ; pSMAD1/5/8 ; pH3
Mouse - E11.5
C
YAP-ir (a.u)
Apical
Basal
D
pS1/5/8-ir (a.u)
E
r=0.71
pS1/5/8-ir (a.u)
F
Ctrl
sh-S1/5
Chick - E4
YAP ; GFP ; pH3
G
Nuclear YAP-ir (pH3+EP+/pH3+;EP-)
H
+/+
+/-
Mouse - E11.5
pYAP ; YAP
I
pYAP-ir/YAP-ir
J
Ctrl + YAP
sh-S1 + YAP
Chick - E5
SOX2 ; HuC/D; GFP
K
Sox2+;HuC/D+
Sox2+;HuC/D-
Sox2-;HuC/D+
Marker+/EP+ (%)
YAP:
L
RGCs / EP+ (%)
M
TBR2+ / EP+ (%)
N
Ectopic SOX2+/EP+ (%)
Alone
+ YAP
O
RGC
IPC
N
VZ

Figure 6

Figure 6: SMAD1/5 regulate early cortical neurogenesis through YAP.

(A) Upon BMP activity, SMAD1/5 are activated and can physically interact and act synergistically with YAP. When SMAD1/5 activity is reduced or abrogated, YAP is inactivated and primed for proteosomal degradation. (B) Expression of YAP during early mouse corticogenesis (E11.5), relative to SMAD1/5 activity (pSMAD1/5/8). The mean intensity ± s.d. of endogenous YAP (C) and pSMAD1/5/8 (D) immunoreactivity was quantified in 70 apical and 28 basal pH3+ mitotic nuclei, obtained from 3 embryos and (E) the correlation between their intensities assessed by the Pearson's correlation coefficient r. (F) Immunostaining of the developing chick cerebral cortex for total YAP 24 hours after IOE with a control or sh-S1/5 plasmid and (G) its mean ratio ± s.d. quantified in electroporated relative to non-electroporated mitotic cells obtained from 7 embryos (Ctrl: 147 pH3+;GFP+ cells and 154 pH3+;GFP- cells, sh-S1/5: 162 pH3+;GFP+ cells and 140 pH3+;GFP- cells). (H) Immunostaining of pYAP and total YAP and (I) quantification of the pYAP/YAP intensity ratio ± s.d. in the developing cerebral cortex of E11.5 SmadNes mutant embryos and control littermates, obtained from 4 embryos (12 sections) per genotype. The normality was tested using the values of individual sections. (J-N) Immunostaining (J) and mean proportion ± s.e.m (K-N) of SOX2+/-;HuC/D+/- cells (K), RGCs (PAX6+;TBR2- cells, L), TBR2+ cells (M) and ectopic SOX2+ cells (N) among electroporated (GFP+) cells 48 hours after IOE of a wild type YAP1 construct (YAP) together with sh-S1 or its control, obtained from n=8-9 embryos per condition. (O) Model proposing that upon BMP signalling, the activated SMAD1/5 recruit YAP to promote RGC self-amplification. When SMAD1/5 activity is reduced or abrogated and YAP is inactivated and primed for degradation, their transcriptional activity is suppressed, thereby enabling RGCs to undergo neurogenic divisions. Significance was assessed with the non-parametric Mann–Whitney test (C, D, G), the two-sided unpaired t-test (I) or a two-way ANOVA + Tukey's multiple comparisons test (K-N). *P<0.05, **P<0.01, ***P<0.001. Scale bars, 50 µm. See also Figure S8.

Supplemental Information

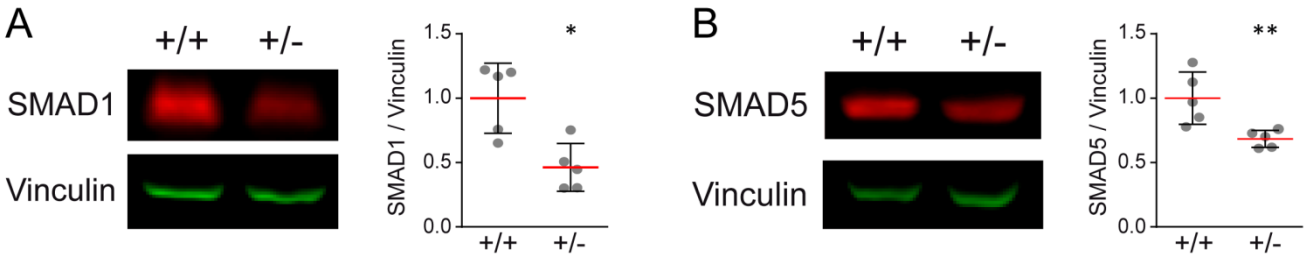

Figure S1: Reduction in SMAD1/5 protein levels in the SmadNes heterozygous mutant mice.

(A-B) The levels of SMAD1 (A) and SMAD5 (B) proteins were assessed by Western blot in extracts obtained from telencephalons of E11.5 SmadNes mutant embryos (+/-) and control littermates (+/+), relative to the levels of Vinculin. The data represent the mean ratio ± s.d obtained from 5 mutant embryos and 5 control littermates. Significance was assessed with the non-parametric Mann–Whitney test (A, B). *P<0.05, **P<0.01.

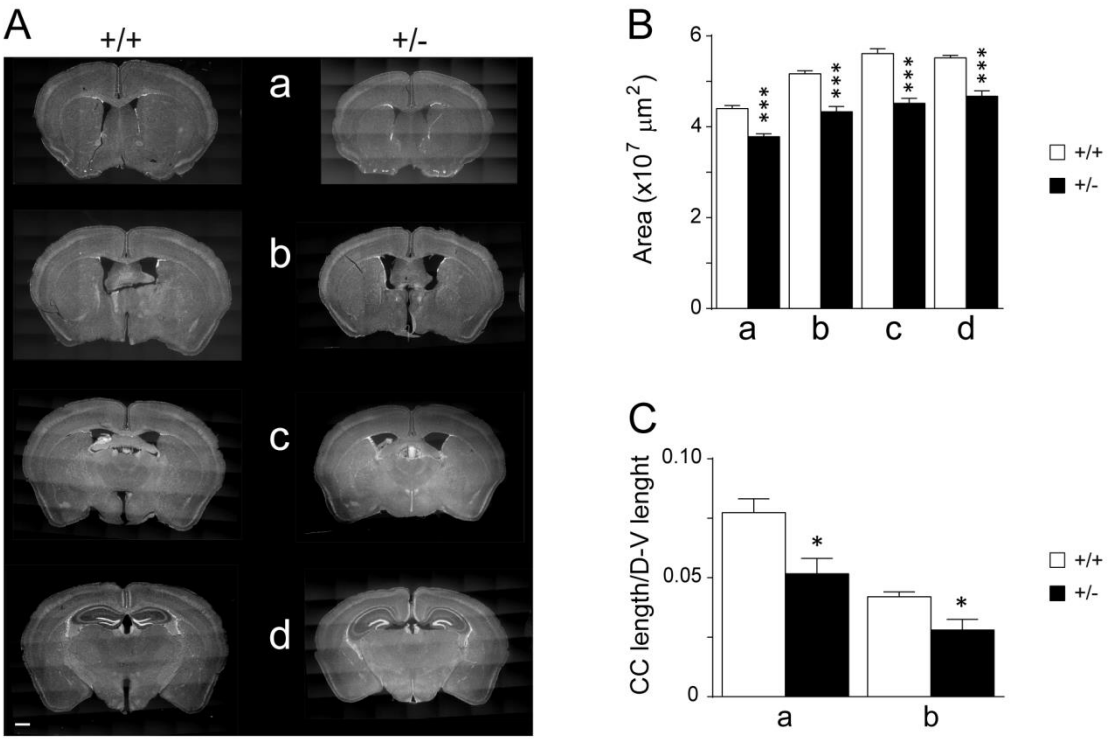

Figure S2: The SmadNes heterozygous mutant mice present microcephaly.

(A) Representative images of the adult (P60) brain of the SmadNes heterozygous mutant mice (+/-) and their control littermates (+/+) in 4 different positions along the rostral-caudal axis (a to d, from rostral to caudal; a is also shown in Fig.1F) and (B) their mean area ± s.e.m, obtained from 3-5 embryos per genotype. (C) The thickness of the corpus callosum of the adult brain of SmadNes mutants and control littermates was measured in coronal sections in 2 different positions (a and b) along the rostral-axis, relative to whole dorsal-ventral (D-V) length. The data represent the mean ratio ± s.e.m obtained from 5 control and 3 mutant mice. Significance was assessed with a two-way ANOVA + Sidak's test (B) or the non-parametric Mann–Whitney test (B). *P<0.05, **P<0.01, ***P<0.001. Scale bars: 500 µm (C).

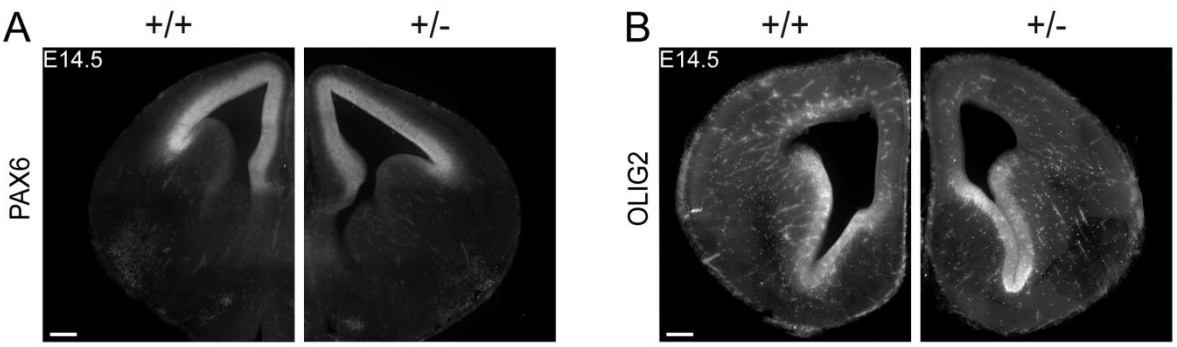

Figure S3 : Absence of patterning defects in the cerebral cortex of SmadNes mutant embryos.

(A, B) Coronal sections showing PAX6 (A) and OLIG2 (B) immunostaining in the telencephalon of E14.5 SmadNes mutant embryos (+/-) and control littermates (+/+). No obvious alteration in the expression domains of these pallial (PAX6) and sub-pallial (OLIG2) patterning markers was observed in the telencephalon of the SmadNes mutant embryos. Scale bars, 100 µm.

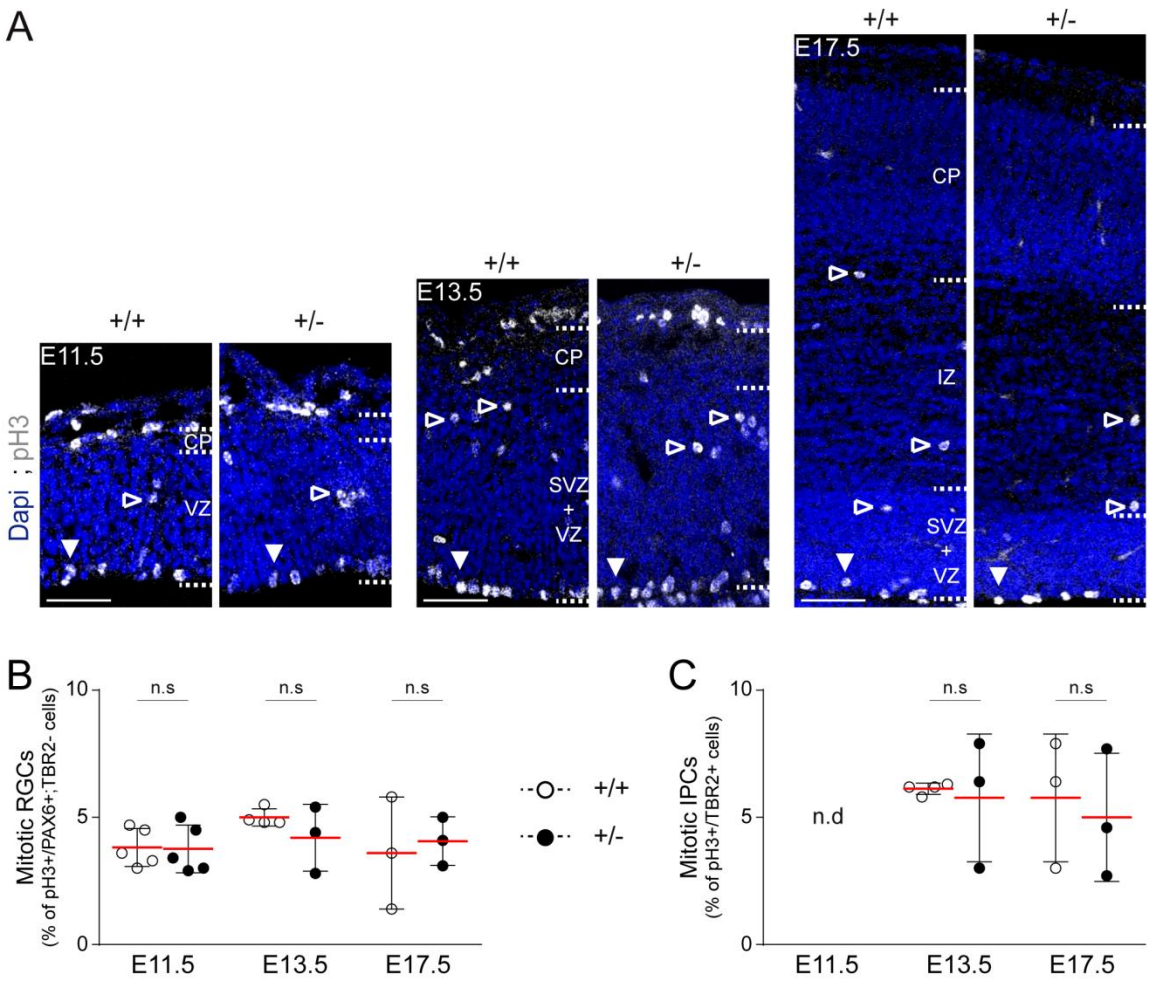

Figure S4: The mitotic index of RGCs and IPCs is not altered in the cerebral cortex of SmadNes mutant embryos.

(A) Coronal sections showing apical (white arrowheads) and basal (black arrowheads) pH3+ mitoses in the developing cerebral cortex of SmadNes mutant embryos (+/-) and control littermates (+/+) at E11.5, E13.5 and E17.5. (B, C) The data represent the mean proportion ± s.d of (B) pH3+/PAX6+;TBR2- cells (mitotic RGCs) and (C) pH3+/TBR2+ cells (mitotic IPCs) counted in a 100 µm-wide radial column unit of the developing cerebral cortex of SmadNes mutant and control littermates embryos, obtained from 3-5 embryos per genotype and stage. The normality was tested using the values of individual sections. Significance was assessed at each developmental stage with the two-sided unpaired t-test. NS: not significant. nd: not determined. Scale bars, 50 µm. CP: cortical plate, IZ: intermediate zone, SVZ: sub-ventricular zone, VZ: ventricular zone.

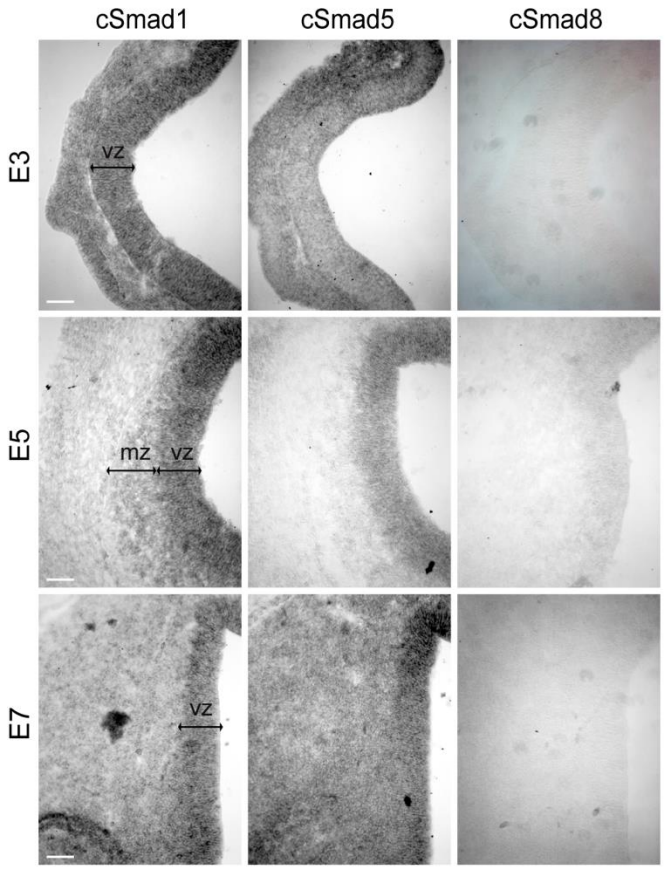

Figure S5: Expression of cSmad1/5/8 during chick cortical neurogenesis.

Coronal sections showing cSmad1, cSmad5 and cSmad8 transcripts detected by in situ hybridization in the developing cerebral cortex of E3, E5 and E7 chick embryos. Scale bars: 50 µm. VZ: ventricular zone, MZ: mantle zone.

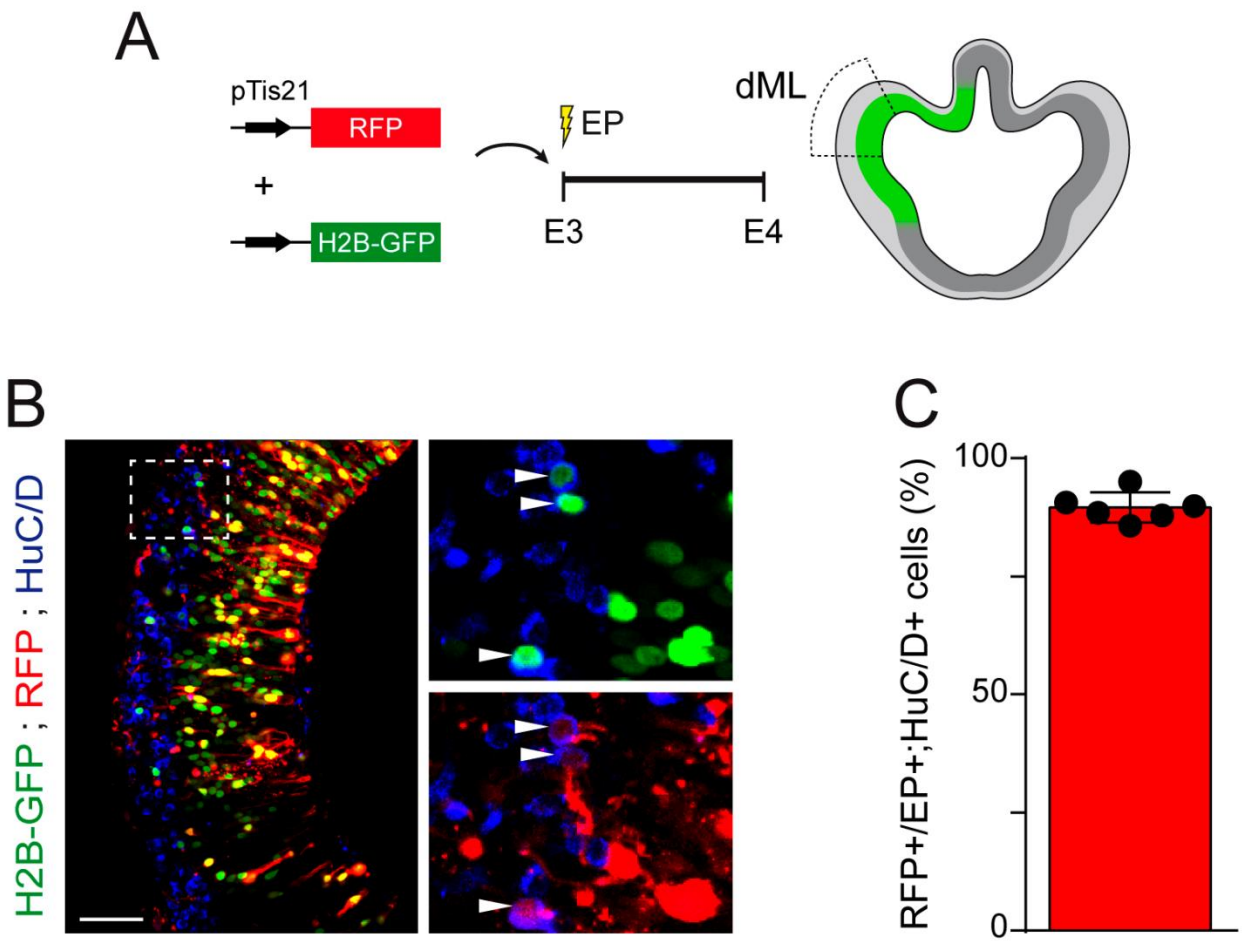

Figure S6: The activity of the pTis21:RFP reporter identifies neurogenic divisions during early chick cortical neurogenesis.

(A) Representation of the methodology used to identify neurogenic divisions during early chick cortical neurogenesis. The pTis21:RFP reporter was co-electroporated together with a constitutively active H2B-GFP-producing plasmid, and its activity assessed in the dorsal medial-lateral (dML) cortical region 24 hours after in ovo electroporation (IOE) of the dorsal telencephalon of E3 chick embryos. (B) Representative image of pTis21:RFP+ cells among the electroporated (H2B-GFP+) cells that differentiated into HuC/D+ neurons 24 hours later and (C) its quantification, presenting the mean proportion of RFP+ cells among H2B-GFP+;HuC/D+ cells ± s.d, obtained from 6 electroporated embryos. Scale bars: 50 µm.

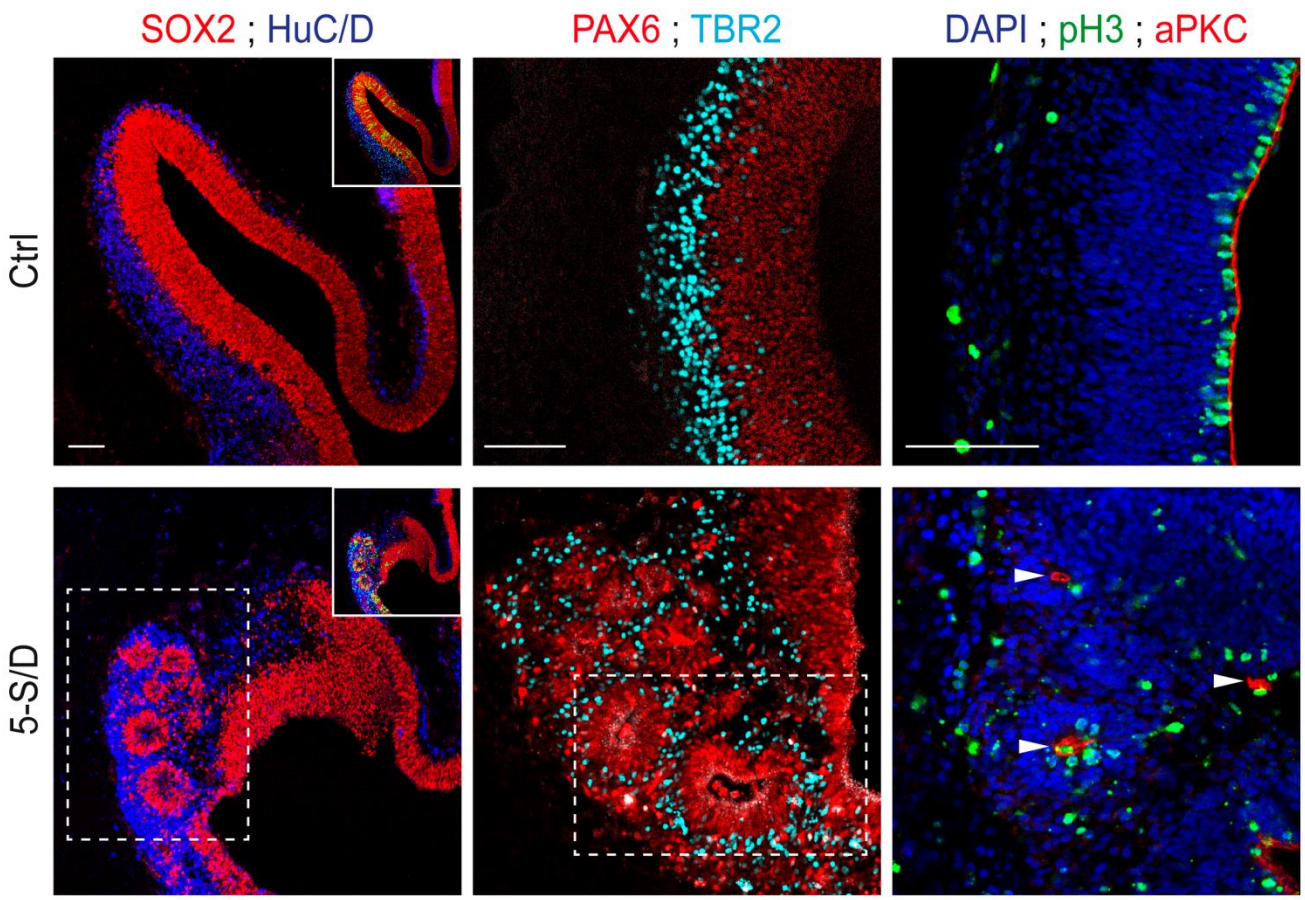

Figure S7: increasing SMAD5 activity causes the abnormal generation of ectopic rosettes of cortical progenitors.

Representative images showing that IOE of SMAD5-S/D can cause the abnormal generation of ectopic rosettes of SOX2+ cortical progenitors. The PAX6+ and TBR2+ cells forming these rosettes developed an ectopic apical-basal polarity, as revealed by immunostaining for the apical marker atypical PKC (aPKC, arrowheads), and divide mostly at the center of the rosettes (pH3+). This phenotype has been observed in the cerebral cortex of 25% (5 out of 20) of the embryos electroporated with SMAD5-SD. Scale bars: 50 µm.

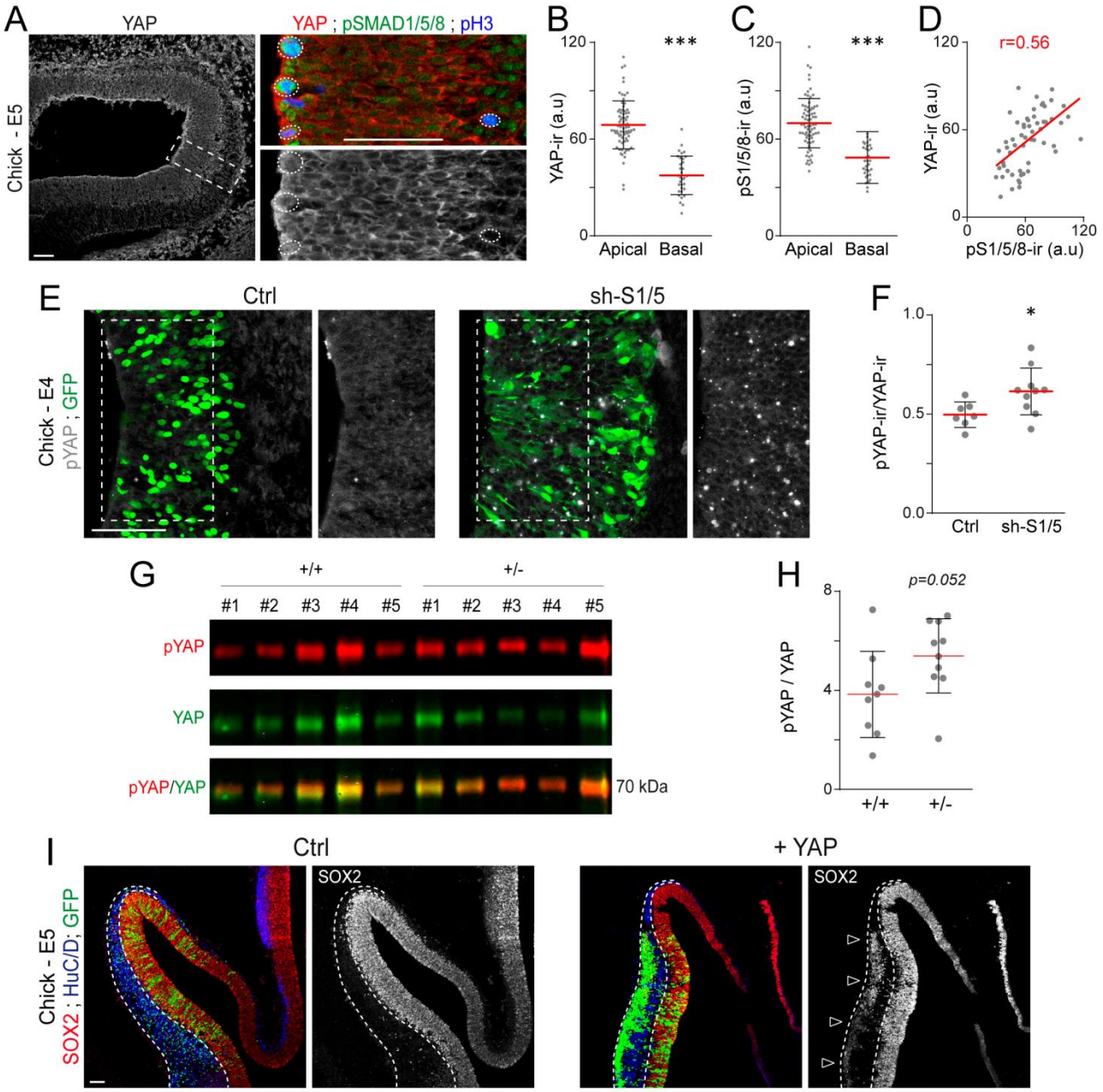

Figure S8: SMAD1/5 regulate early cortical neurogenesis through YAP.

(A) Expression of YAP during chick corticogenesis, relative to SMAD1/5 activity (pSMAD1/5/8). (B,C) The mean intensity ± s.d of endogenous YAP (B) and pSMAD1/5/8 (C) immunoreactivity was quantified in 74 apical and 33 basal mitotic (pH3+) nuclei obtained from 3 chick E5 embryos. (D) The correlation between the intensity of endogenous pSMAD1/5/8 and YAP immunoreactivities was assessed by calculating the Pearson's correlation coefficient r. (E) Immunostaining of the form of YAP

phosphorylated at Serine 123 (pYAP) and (F) quantification of the mean ratio ± s.d of pYAP/YAP intensity obtained 24 hours after IOE with sh-S1/5 (10 sections from 3 embryos) or its control (7 sections from 3 embryos). (G) Western blot detection of the levels of pYAP and total YAP in extracts obtained from telencephalons of E11.5 SmadNes mutant embryos (+/-) and control littermates (+/+). (H) Quantification of the mean pYAP/YAP ratio ± s.d, obtained from 10 SmadNes mutant embryos (+/-) and 9 control littermates (+/+) derived from 2 different litters. (I) Immunostaining of the developing chick cerebral cortex for SOX2+ neural progenitors and HuC/D+ differentiating neurons 48 hours after IOE with a construct overexpressing the wild type form of YAP (YAP) or a control, showing that YAP overexpression can lead to a massive ectopic delamination of SOX2+ electroporated cells in the basal part of the mantle zone. Significance was assessed with the non-parametric Mann–Whitney test (B, C, F), the two-sided unpaired t-test (D, H).*P<0.05, ***P<0.001. Scale bars, 50 µm.

Reference	Function	Gene	base Mean Exp	padj	mut/wt (log2FC)
ENSMUSG00000055320.17,Tead1,protein_coding	Transcription factor	Tead1	9332,54	0,9999886	0,101210746
ENSMUSG00000030796.17,Tead2,protein_coding	Transcription factor	Tead2	9672,80	0,9999886	0,024821616
ENSMUSG00000002249.19,Tead3,protein_coding	Transcription factor	Tead3	1047,61	0,9999886	0,033058565
ENSMUSG00000053110.13,Yap1,protein_coding	Transcriptional co-factor	Yap1	4306,39	0,9999886	0,081556333
ENSMUSG00000009995.17,Taz,protein_coding	Transcriptional co-factor	Taz1	1137,68	0,9999886	0,008523141
ENSMUSG00000040021.13,Lats1,protein_coding	Kinase	Lats1	5782,05	0,9999886	0,062499988
ENSMUSG00000021959.16,Lats2,protein_coding	Kinase	Lats2	945,26	0,9999886	0,058998692
ENSMUSG00000018209.15,Stk4,protein_coding	Kinase	Mst1/Stk4	3337,43	0,9999886	-0,002528479
ENSMUSG00000022329.14,Stk3,protein_coding	Kinase	Mst2/Stk3	810,49	0,9999886	0,034100011
ENSMUSG00000043131.14,Mob1a,protein_coding	Transduction signaling	Mob1a	3301,95	0,9999886	-0,009675482
ENSMUSG00000006262.15,Mob1b,protein_coding	Transduction signaling	Mob1b	4133,62	0,9999886	0,103089689
ENSMUSG00000009073.16,Nf2,protein_coding	Transduction signaling	Nf2	6091,92	0,9999886	-0,062201005
ENSMUSG00000048285.9,Frmd6,protein_coding	Transduction signaling	Frmd6	578,75	0,9999886	-0,03610473
ENSMUSG00000036862.15,Dchs1,protein_coding	Cadherin	Dchs1	18275,80	0,9999886	-0,045231061
ENSMUSG00000046743.6,Fat4,protein_coding	Cadherin	Fat4	11600,80632	0,9999886	0,036515018

Table S2: Expression of the genes of the Hippo signalling pathway in cortical RGCs from SmadNes mutant and control E12.5 embryos.

The list of genes belonging to the mouse Hippo signaling pathway was defined based on KEGG pathways (https://www.genome.jp). The genes are presented according to their function. Their expression was quantified by genome-wide RNA-seq in RNA samples obtained from cortical RGCs from SmadNes mutant and control E12.5 embryos purified by FACS based on their Prominin1 expression. Their expression levels (base mean exp), differential expression in mutant vs control samples (mut/wt, expressed in Log2) and the corresponding adjusted p-value are shown. The genes whose transcripts could not be detected by RNA-seq or whose expression levels are below the defined treshold (<100) were not included (Tead4, Frmd1, Dchs2).

REAGENT or RESOURCE	**SOURCE**	IDENTIFIER
Antibodies		
anti-aPKC (mouse)	Santa Cruz Biotechnologies	Cat #SC-17781 (H-1) RRID:AB_628148
anti-BrdU (rat)	AbD Serotec	Cat #MCA2060 RRID:AB_323427
anti-pHistone3 (rat)	Sigma Aldrich	Cat #H9908 RRID:AB_260096
anti-HuC/D (mouse)	Life Technologies	Cat #A-21271 RRID:AB_221448
anti-MEF2c (rabbit)	Abcam	Cat#ab64644 RRID:AB_2142861
anti-NeuN (mouse)	Millipore	Cat # MAB377 RRID: AB_2298772
anti-OLIG2 (rabbit)	Millipore	Cat#AB9610 RRID: AB_570666
anti-PAX6 (mouse)	DSHB	Cat#pax6 RRID:AB_528427
anti-PAX6 (rabbit)	Covance / Biolegend	Cat #901301 RRID:AB_2565003
anti-Prominin1 (rat)	eBioscience	Cat #17-1331-81 RRID: AB_823120
anti-SMAD1 (rabbit)	Cell Signaling Technologies	Cat #6944S RRID:AB_10858882
anti-SMAD5 (rabbit)	Cell Signaling Technologies	Cat # 12534S RRID: n.d
anti-pSMAD1/5/8 (rabbit)	Cell Signaling Technologies	Cat#9511 RRID:AB_331671
anti-SOX2 (rabbit)	Abcam	Cat #ab97959 RRID:AB_2341193
anti-TBR1 (rabbit)	Abcam	Cat #ab31940 RRID:AB_2200219
anti-TBR2 (rabbit)	Abcam	Cat #ab23345 RRID:AB_778267
anti-TUBULIN-b3 (Tuj1) (mouse)	Covance	Cat #MMS-435P RRID:AB_2313773
anti-Vinculin (mouse)	Sigma	Cat # V9131 RRID: AB_477629
anti-YAP (mouse)	Santa Cruz Biotechnologies	Cat # sc-101199 RRID:AB_1131430
anti-pYAP (rabbit)	Cell Signaling Technologies	Cat#4911 RRID:AB_2218913

Table S3: List of primary antibodies used in this study.